

Article

Entropy Analysis in MHD CNTS Flow Due to a Stretching Surface with Thermal Radiation and Heat Source/Sink

K. N. Sneha¹, U. S. Mahabaleshwar^{1,*}, Mohsen Sharifpur^{2,3,*}, Mohammad Hossein Ahmadi^{4,*}
and Mohammed Al-Bahrani⁵

- ¹ Department of Studies in Mathematics, Shivagangothri, Davangere University, Davangere 577007, India
² Department of Mechanical and Aeronautical Engineering, University of Pretoria, Pretoria 0002, South Africa
³ Department of Medical Research, China Medical University Hospital, China Medical University, Taichung 404, Taiwan
⁴ Faculty of Mechanical Engineering, Shahrood University of Technology, Shahrood 3619995161, Iran
⁵ Chemical Engineering and Petroleum Industries Department, Al-Mustaqbal University College, Babylon 51001, Iraq
* Correspondence: u.s.m@davangereuniversity.ac.in (U.S.M.); mohsen.sharifpur@up.ac.za (M.S.); mohammadhosein.ahmadi@gmail.com (M.H.A.)

Abstract: The consequence of magnetohydrodynamics (MHD) flow on entropy generation analysis and thermal radiation for carbon nanotubes via a stretched surface through a magnetic field has been discovered. The governing partial differential equations are altered into ordinary differential equations with the aid of the similarity variable. Here, water is considered the base fluid with two types of carbon nanotubes, such as single-wall carbon nanotubes (SWCNTs) and multi-wall carbon nanotubes (MWCNTs). This domain is used in the energy equation, and then it is solved analytically and transferred in terms of hypergeometric function. The existence and nonexistence of solutions for stretching are investigated. Some of the primary findings discussed in this article show that the presence of carbon nanotubes, magnetic field, and Eckert number develop heat transfer in nanofluids and heat sources and that Eckert number reduces entropy formation. Different regulating parameters, such as Casson fluid, mass transpiration, thermal radiation, solid volume fractions, magnetic constraint, and heat source/sink constraint, can be used to analyze the results of velocity and temperature profiles. The novelty of the current study on the influence of magnetic field entropy analysis on CNTs flow with radiation, is that elastic deformation is the subject of this research, and this has not previously been examined. Higher values of heat sources and thermal radiation enhance the heat transfer rate. The study reveals that thermal radiation, Casson fluid; mass transpiration, Darcy number, and Prandtl number increase, and that decrease in the buoyancy ratio, magnetic parameter, and volume fraction decrease the values of the buoyancy ratio, and also control the transfer of heat.

Keywords: MHD; CNTs; entropy generation; thermal radiation; heat source/sink

MSC: 76W05



Citation: Sneha, K.N.; Mahabaleshwar, U.S.; Sharifpur, M.; Ahmadi, M.H.; Al-Bahrani, M. Entropy Analysis in MHD CNTS Flow Due to a Stretching Surface with Thermal Radiation and Heat Source/Sink. *Mathematics* **2022**, *10*, 3404. <https://doi.org/10.3390/math10183404>

Academic Editor: James M. Buick

Received: 2 August 2022

Accepted: 11 September 2022

Published: 19 September 2022

Publisher's Note: MDPI stays neutral with regard to jurisdictional claims in published maps and institutional affiliations.



Copyright: © 2022 by the authors. Licensee MDPI, Basel, Switzerland. This article is an open access article distributed under the terms and conditions of the Creative Commons Attribution (CC BY) license (<https://creativecommons.org/licenses/by/4.0/>).

1. Introduction

Theoretical fluid mechanics encompasses a wide range of properties and processes. The processes revolving around the laminar boundary layer, both in steady and unstable circumstances, have a lot of weight in the field of aerodynamics development. Polymer extrusion techniques, linear and nonlinear stretching processes, glass and sheet cooling methods, hydronautics, biofluid dynamics, and numerous manufacturing-related applications are also evolving (see Fisher [1]). The complexity of stretching sheet research is enormously important, and it applies to a variety of real-world applications, including metallurgy and polymer extrusion. These processes are frequently observed in applications, such as continuous stretching and rolling in metal forming, annealing in some heat treatment procedures, and also in the production of polymer sheets, the cooling of long plates,

particularly metallic, and the flow of a boundary layer during condensation processes, as well as the flow of a liquid film during compression methods. These approaches have sparked research into boundary layer flow phenomena on a stretching sheet. Improving energy transfer efficiency and energy conservation are becoming more difficult as a result of the world's rapid advancement in science and technology. However, one of the most frequently used strategies for improving heat transmission is the use of new materials with better characteristics. Traditional heat transfer fluids, like engine oil, water, or ethylene glycol, are unable to meet the demands for robust heat transmission and micro cooling. Meanwhile, the development of cooling technology and high-efficiency heat transfer has been severely hampered by the restricted heat transfer capacities of the current heat transfer medium, based on their thermophysical properties. For instance, when used properly, solar energy, one of the most abundant exploitable renewable energy sources, may sufficiently meet the world's energy needs. However, low solar energy conversion and poor collection, are major barriers to using solar energy.

Bhattacharyya et al. [2] are pioneers in addressing the problem of stretching sheets. A research study by Mabood et al. [3] outlined the impact of melting on MHD Casson fluid flow past a stretching sheet in a porous medium with radiation. Crane [4] extended this work with fluid flow over a stretching/shrinking surface. Many studies on stretching sheet problems are being conducted as a result of these works. Andersson et al. [5] studied the magnetohydrodynamic flow of a power-law fluid over a stretching sheet. Andersson et al. [6] studied the MHD flow of a viscoelastic fluid past a stretching surface. Fang et al. [7] investigated the closed-form exact solutions of MHD viscous flow over a shrinking sheet. Abolbashari et al. [8] investigated the analytical modeling of entropy generation for Casson nano-fluid flow induced by a stretching surface. Souayeh et al. [9] conducted a comparative analysis on non-linear radiative heat transfer on MHD Casson nanofluid past a thin needle.

Magnetic field is one of the most critical factors in determining the rate of cooling and the desired quality of the industrial field. Using a magnetic field, many investigations can be carried out. Abdul et al. [10] studied heat and velocity problems with different fluids and conditions under the influence of a magnetic field. Aly et al. [11,12] studied the influence of inclined Lorentz forces on the boundary layer flow of Casson fluid over an impermeable stretching sheet with heat transfer. Apart from these studies, researchers have tried to investigate the stretching problem differently, using different fluids. Anusha et al. [13] studied the MHD of nanofluid flow over a porous stretching/shrinking plate with mass transpiration and Brinkman ratio. Kumaran et al. [14] investigated Thermophoresis and Brownian moment effects on the parabolic flow of MHD Casson and Williamson fluids with cross-diffusion.

Additionally, the physical properties of a base fluid can be altered by suspending nanoparticles of the desired metal in the fluid, so one gets what is called a nanofluid. A special kind of nanoparticle is the carbon nanotube (CNT). These kinds of solids were first discovered by Iijima [15] in his study of carbon nanotubes (CNTs). CNTs are a well-known allotrope of the fullerene family exhibiting a long and hollow chemical structure, comprising graphene sheets. In a broader sense, two kinds of CNTs exist, viz., single and multiwalled. One can also find, in the literature, many applications where they can be used, e.g., wastewater treatment, petroleum transportation, power plant piping, and combustion. Khan et al. [16] conducted a heat transfer analysis of MHD water functionalized carbon nanotube flow over a static/moving wedge. Anuar et al. [17] studied the mixed convection flow and heat transfer of carbon nanotubes over an exponentially stretching/shrinking sheet with suction and slip effect. Khan et al. [18] investigated the fluid flow and heat transfer of carbon nanotubes along a flat plate with Navier slip boundary. Shalini et al. [19] examined the unsteady MHD chemically reacting mixed convection nano-fluids flow past an inclined porous stretching sheet with slip effect and variable thermal radiation and heat source. Yana et al. [20] inspected the inclined Lorentz force impact on convective-radiative heat exchange of micropolar nanofluid inside a porous enclosure with tilted elliptical heater.

The effect of MHD, mass transpiration, and Casson fluid parameters on the flow was analyzed. Many authors have demonstrated the significance of non-Newtonian rheological models. Mukhopadhyay and Vajravelu [21] studied the diffusion of chemically reactive species in Casson fluid flow over an unsteady permeable stretching surface. Sankar and Lee [22] examined the two-fluid Casson model for pulsatile blood flow through stenosed arteries: a theoretical model. Finally, Sneha et al. [23] studied the magnetohydrodynamic flow of a Newtonian fluid over a superliner stretching/shrinking surface and also the existence of mass transpiration and radiation on the MHD flow using CNTs.

Industries, engineering, technology, and everyday activities using heat include the development of entropy. Entropy as the measurement of disturbance in the thermal system and it transforms thermal energy into mechanical work was studied by Bejan [24]. Campfires and the burning of solid wood into ash, smoke, and gases are examples of how entropy is inextricably linked to daily human existence. To minimize energy loss, liquids are handled to maximize their fluid efficiency for thermal applications. Khan et al. [25] examined the entropy generation theory in the thermal environment. Shafee et al. [26] studied entropy generation via convective heat transport as the subject of recent research and also studied the entropy generation analysis for MHD water-based Fe_3O_4 Ferro fluid through a porous semi annulus cavity via cvfem. Many scientists and researchers have looked into seeing how much entropy is generated during the convection process. Entropy production is an issue in diminishing the productivity of engineering organisms, including analysis. Shipping and transmission are dependent on the component's unchangeable circumstances. Coolers, mixing, cap manufacturers, freezers, and steam turbines are examples of entropy modeling approaches. Jamshed et al. [27] examined the Cattaneo–Christov based study of $\text{TiO}_2\text{-CuO}$ /eg Casson hybrid nanofluid flow over a stretching surface with entropy generation. Sindhu and Giresha [28] studied entropy generation analysis of hybrid nanofluid in a microchannel with slip flow, convective boundary and nonlinear heat flux. Khan et al. [29] investigated the irreversibility analysis and heat transport in squeezing nano-liquid flow of non-Newtonian (second-grade) fluid between infinite plates with activation energy. While flow is an issue, the heat source consequence is an essential part of heat transport. Electronic devices, semiconductors, and nuclear reactors are only a few of the physical uses of heat generation/absorption. Mumraiz et al. [30] examined entropy generation in the electrical magnetohydrodynamic flow of $\text{Al}_2\text{O}_3/\text{Cu-H}_2\text{O}$ hybrid nanofluid with non-uniform heat flux. Reddy [31] considered the biomedical aspects of entropy generation on electromagnet hydrodynamic blood flow of hybrid nanofluid with nonlinear thermal radiation and non-uniform heat source/sink. Hayat et al. [32] studied the numerical simulation for nonlinear radiative flow by a convective cylinder.

The novelty of the current study of the influence of magnetic field entropy analysis on the flow of CNTs with radiation, is that elastic deformation is the subject of this research, and this has not previously been examined. Thus, we primarily focus on this aspect of the sheet's stretchable surface, and examine the flowing nature. We analyze non-linear thermal radiation, viscous dissipation, and magnetic field. In the modeling of energy expression, viscous dissipation, heat source/sink, thermal radiation, and elastic deformation influences were used. Herein a comparative study of the SWCNT and MWCNT effect on nanofluid motion is presented. The total entropy rate is calculated. ODEs result from a suitable transformation. For analytical results, the hypergeometric function was used. Different graphs depict the velocity profile, temperature, skin friction coefficient, and entropy generation. Results for CNTs with single and multiple walls were grouped and contrasted. According to our research, the Brinkman number and temperature ratio parameters rose together with entropy generation. Radiative factors became more intense as the temperature rose. Additionally, when compared to MWCNT, the temperature gradient was slightly higher for SWCNT. Ultimately, modeling data is shown to demonstrate the usefulness of the suggested technique and to compare the created findings to certain research work to demonstrate the technique's efficiency. An analytical system solved the nonlinear systems. The performances of many governing flow variables are described

in complete plots. In addition, the difference in some valuable engineering quantities is interpreted via tabular values.

2. Mathematical Analysis and Solution

We explored its potential of generating a Casson fluid flow with nanofluid through an MHD stretching surface with an angled magnetic field. Thermal radiation’s goal is to create non-dimensional objects. In the thermal model, a heat source/sink is also assumed to investigate a transfer in nanoparticles with water as a solvent as their primary fluid. The flow moves with velocity. The flow of the physical model is represented in Figure 1. The strength of the magnetic effect B_0 is taken to be parallel to the y -axis. Fundamental models, which are the governing equations of the present problem, are given by:

$$\frac{\partial u}{\partial x} + \frac{\partial v}{\partial y} = 0 \tag{1}$$

$$u \frac{\partial u}{\partial x} + v \frac{\partial u}{\partial y} = \left(1 + \frac{1}{\Lambda}\right) \nu_{nf} \frac{\partial^2 u}{\partial y^2} - \frac{\sigma_{nf} B_0^2}{\rho_{nf}} \text{Sin}^2 \tau u \tag{2}$$

$$u \frac{\partial T}{\partial x} + v \frac{\partial T}{\partial y} = \frac{\kappa_{nf}}{(\rho C_p)_{nf}} \frac{\partial^2 T}{\partial y^2} - \frac{1}{(\rho C_p)_{nf}} \frac{\partial q_r}{\partial y} + \frac{q'''}{(\rho C_p)_{nf}} + \frac{h_{nf}}{(\rho C_p)_{nf}} \left(\frac{\partial u}{\partial y}\right)^2 + \frac{\sigma_{nf} B_0^2}{(\rho C_p)_{nf}} u^2 \text{Sin}^2 \tau - \frac{\delta k_0}{(C_p)_{nf}} \left[\frac{\partial u}{\partial y} \frac{\partial}{\partial y} \left(u \frac{\partial u}{\partial x} + v \frac{\partial u}{\partial y}\right)\right], \tag{3}$$

Here, u and v represent velocity components, δ is the elastic deformation, the elastic parameter is k_0 , and q''' is heat generation/absorption.

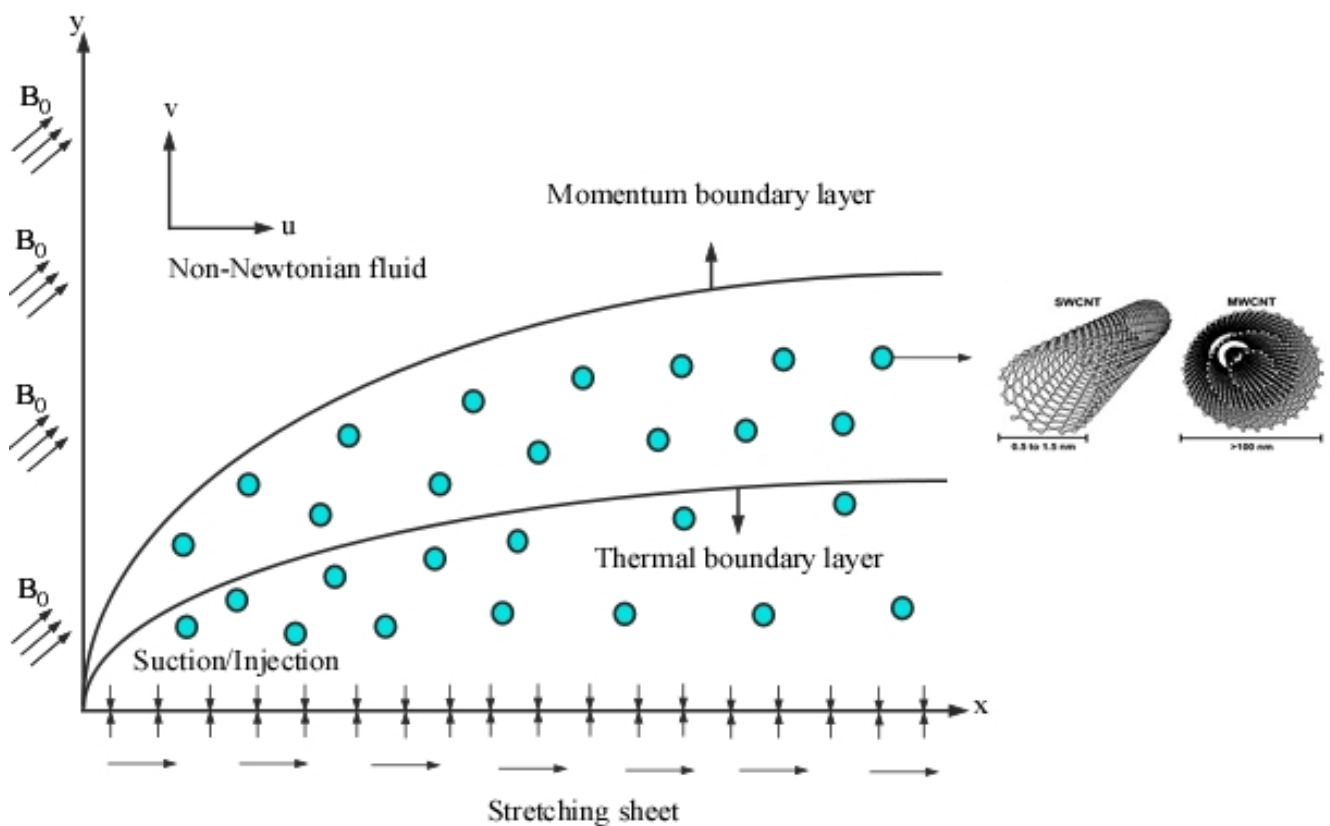


Figure 1. Physical model of coordinate system.

The B. Cs associated with the above equation are given as:

$$\begin{aligned} u &= dax, \quad v = v_w(x), \quad T = T_w = A\left(\frac{x}{l}\right)^2 = T_\infty \quad \text{at } y = 0, \\ u &\rightarrow 0, \quad T \rightarrow T_\infty \quad \text{as } y \rightarrow \infty. \end{aligned} \tag{4}$$

The value of q_r can be defined on the basis of Rosseland’s approximation, as shown (see Sneha et al. [33] and Vishalakshi et al. [34]):

$$q_r = -\frac{4\sigma^*}{3k^*} \frac{\partial T^4}{\partial y}, \tag{5}$$

Ambient temperature T^4 expansion in terms of Taylor’s series is:

$$T^4 = T_\infty^4 + 4T_\infty^3(T - T_\infty) + 6T_\infty^2(T - T_\infty)^2 + \dots \tag{6}$$

Disregarding higher order terms in Equation (6), yields the equation:

$$T^4 = -3T_\infty^4 - 4T_\infty^3T \tag{7}$$

On applying Equation (7) into Equation (5), the first order derivative of heat flux can be given by:

$$\frac{\partial q_r}{\partial y} = -\frac{16\sigma^*T_\infty^3}{3k^*} \frac{\partial^2 T}{\partial y^2}. \tag{8}$$

Suitable similarity transformations are given by:

$$\eta = y\sqrt{\frac{a}{\nu_f}}, \quad u = ax F_\eta(\eta), \quad v = -\sqrt{a\nu_f}F(\eta), \quad \theta(\eta) = \frac{T - T_\infty}{T_w - T_\infty} \tag{9}$$

On using Equations (8) and (9) in Equations (1) to (3) the following ODEs can be derived:

$$\frac{\varepsilon_1}{\varepsilon_2} \left(1 + \frac{1}{\Lambda}\right) F_{\eta\eta\eta} + FF_{\eta\eta} - F_\eta^2 - \frac{\varepsilon_3}{\varepsilon_2} M \text{Sin}^2\tau F_\eta = 0 \tag{10}$$

$$\begin{aligned} \frac{\varepsilon_4}{Pr} (\varepsilon_5 + N_R)\theta_{\eta\eta} + F\theta_\eta + \frac{\varepsilon_5}{\varepsilon_7\varepsilon_2\varepsilon_6 Pr} B^*\theta - 2F_\eta\theta &= -\varepsilon_1\varepsilon_4 Ec F_\eta^2 - \frac{\varepsilon_5}{\varepsilon_7\varepsilon_2\varepsilon_6 Pr} A^*F_\eta \\ &- \delta k_1\varepsilon_6 Ec [F_\eta F_{\eta\eta} + FF_{\eta\eta\eta}] \end{aligned} \tag{11}$$

Boundary conditions associated with these equations also reduce to:

$$\left. \begin{aligned} F_\eta(\eta) &= d, \quad F(\eta) = V_C, \quad \theta(\eta) = 1, \quad \text{at } \eta = 0, \\ F_\eta(\eta) &\rightarrow 0, \quad \theta(\eta) \rightarrow 0 \quad \text{as } \eta \rightarrow \infty. \end{aligned} \right\} \tag{12}$$

Here, $M = \frac{\sigma_f B_0^2}{\rho_f a}$ is the magnetic parameter, $Ec = \frac{a^2 l}{A(C_p)_f}$ is the Eckert number, and the Prandtl number is $Pr = \frac{(\rho C_p)_f \nu_f}{\kappa_f}$, $q''' = \left(\frac{\kappa_{nf} u_w(x)}{x\nu_{nf}}\right) [A^*(T_w - T_\infty)f_\eta + B^*(T - T_\infty)]$. $A^*, B^* > 0$ reflects heat production, $A^*, B^* < 0$ heat absorption, and $V_C = -\frac{v_w}{\sqrt{av}}$ mass transpiration. If $V_C > 0$ this indicates suction, and $V_C < 0$ indicates injection. $N_R = \frac{16\sigma^* T_\infty^3}{3k^* \kappa_f}$ is the thermal radiation, $\varepsilon_1 = \frac{\mu_{nf}}{\mu_f}$, $\varepsilon_2 = \frac{\rho_{nf}}{\rho_f}$, $\varepsilon_3 = \frac{\sigma_{nf}}{\sigma_f}$, $\varepsilon_4 = \frac{(\rho C_p)_{nf}}{(\rho C_p)_f}$, $\varepsilon_5 = \frac{\kappa_{nf}}{\kappa_f}$, $\varepsilon_6 = \frac{(C_p)_f}{(C_p)_{nf}}$, $\varepsilon_7 = \frac{\nu_{nf}}{\nu_f}$, and $K_1 = \frac{k_0 x}{a}$ is elastic deformation.

Where ϕ describes the solid volume fraction, the sub-scripts nf and “CNT” are used for the base fluid and carbon nanotubes, respectively. The thermophysical properties of water and carbon nanotubes are given in Tables 1 and 2.

Table 1. Proposed nanofluid models. Khan et al. [18], Xue [35].

Nanofluid Properties	
$\epsilon_2 = \rho_{nf} = (1 - \phi)\rho_f + \phi \rho_{CNT}$	
$\epsilon_1 = \mu_{nf} = \frac{\mu_f}{(1-\phi)^{2.5}}$	
$\epsilon_4 = (\rho C_p)_{nf} = (1 - \phi)(\rho C_p)_f + \phi(\rho C_p)_{CNT}$	
$\epsilon_5 = k_{nf} = \left[\frac{(1-\phi)+2\phi\left(\frac{k_{CNT}}{k_{CNT}-k_f}\right)\ln\left(\frac{k_{CNT}+k_f}{2k_f}\right)}{(1-\phi)+2\phi\left(\frac{k_f}{k_{CNT}-k_f}\right)\ln\left(\frac{k_{CNT}+k_f}{2k_f}\right)} \right] k_f$	
$\epsilon_3 = \sigma_{nf} = \left[1 + \frac{3(\sigma_{CNT}-\sigma_f)\phi}{(\sigma_{CNT}+2\sigma_f)-(\sigma_{CNT}-\sigma_f)\phi} \right] \sigma_f$	

Table 2. Properties of each phase. Anuar [36].

Properties	SWCNT	MWCNT	H ₂ O
$\rho(kgm^{-3})$	425	796	997
$C_p(Jkg^{-1}K^{-1})$	2600	1600	4179
$k(Wm^{-1}K^{-1})$	6600	3000	0.613
$\sigma(\Omega^{-1}m^{-1})$	48,000,000	38,000,000	0.05
$\mu(\times 10^{-5}Pas)$			

Analytical solution for momentum equation.

Let us assume the solution of Equations (10) and (12) is of the form:

$$F(\eta) = V_C + \frac{d}{\lambda}(1 - Exp(-\lambda\eta)) \tag{13}$$

Using this solution (13) in Equation (10) derives the following quadratic equation:

$$\frac{\epsilon_1}{\epsilon_2} \left(1 + \frac{1}{\Lambda} \right) \lambda^2 - V_C \lambda - \left(d + \frac{\epsilon_3}{\epsilon_2} M Sin^2\tau \right) = 0 \tag{14}$$

Solving this quadratic equation derives the solution domain λ as:

$$\lambda = \frac{V_C \epsilon_2 + \sqrt{(2V_C \epsilon_2)^2 - \left(d + \frac{\epsilon_3}{\epsilon_2} M Sin^2\tau \right) \frac{\epsilon_1}{\epsilon_2} \left(1 + \frac{1}{\Lambda} \right)}}{2 \frac{\epsilon_1}{\epsilon_2} \left(1 + \frac{1}{\Lambda} \right)} \tag{15}$$

and the velocity becomes:

$$F_{\eta\eta}(\eta) = -d\lambda Exp(-\lambda\eta) \tag{16}$$

To extend the results of this study, consider the term, defined as:

$$\sqrt{Re_x} C_f = \frac{\tau_w}{\rho_f u_w^2} = \frac{\epsilon_1}{\epsilon_2} \left(1 + \frac{1}{\Lambda} \right) f_{\eta\eta}(0) \tag{17}$$

Here, $Re_x = \frac{ax^2}{\nu_f}$ is called the local Reynolds's number.

3. Analytical Solution for Energy Equation

To get the results of Equation (13), we define the following variable ζ as follows:

$$\zeta = -\frac{dPr}{\omega\lambda^2} Exp(-\lambda\eta) \tag{18}$$

Substituting this new variable, defined in Equation (18), into Equation (11) derives the following equation:

$$\zeta \frac{\partial^2 \theta}{\partial \zeta^2} + (1 + A_0 - \zeta) \frac{\partial \theta}{\partial \zeta} - \frac{\epsilon_5}{\epsilon_7 \epsilon_2 \epsilon_6 d Pr [Exp(-\lambda\eta)]} B^* \theta - 2\theta = \epsilon_1 \epsilon_4 Ec d \lambda^2 [Exp(-\lambda\eta)] + \frac{\epsilon_5}{\epsilon_7 \epsilon_2 \epsilon_6 Pr} A^* d [Exp(-\lambda\eta)] + \delta k_1 \epsilon_6 Ecd \lambda^2 [Exp(-\lambda\eta)] (V_c \lambda + d) \tag{19}$$

In the above equation,

$$A_0 = \frac{Pr l}{\omega \lambda^2}, \quad l = (V_c \lambda - d), \quad \omega = \varepsilon_4(\varepsilon_5 + N_R)$$

The boundary conditions associated with Equation (18) also reduce to:

$$\theta \left(-\frac{dPr}{\omega \lambda^2} \text{Exp}(-\lambda \eta) \right) = 1, \quad \theta(0) = 0. \tag{20}$$

by using the solutions expressed in Equation (20) in the Equation (19) the following analytical solutions are derived:

$$\theta(\eta) = h_1 \text{Exp}[-m_1 \lambda \eta] F \left(m_1 - 2, B_0 + 1, -\frac{dPr}{\omega \lambda^2} \text{Exp}(-\lambda \eta) \right) + h_2 \text{Exp}(-\lambda \eta) + h_3 \text{Exp}(-2\lambda \eta) \tag{21}$$

$$\theta_\eta(0) = -h_1 \frac{A_0+B_0}{2} \lambda F \left(\frac{A_0+B_0}{2} - 2, B_0 + 1, -\frac{dPr}{\omega \lambda^2} \right) + h_1 \frac{A_0+B_0-4}{2(1+B_0)} \frac{dPr}{\omega \lambda} F \left(\frac{A_0+B_0}{2} - 1, B_0 + 2, -\frac{dPr}{\omega \lambda^2} \right) - h_2 \lambda - 2\lambda h_3. \tag{22}$$

where,

$$m_1 = \frac{-A_0+B_0}{2}, \quad B_0 = \sqrt{a_0^2 - \frac{4\varepsilon_5 B^*}{\varepsilon_7 \varepsilon_2 \varepsilon_6 \omega \lambda^2}},$$

$$h_1 = \frac{1-(h_2+h_3)}{F \left(m_1-2, b_0+1, -\frac{dPr}{\omega \lambda^2} \text{Exp}(-\lambda \eta) \right)}, \quad h_2 = -\frac{d\varepsilon_5 A^*}{\varepsilon_7 \varepsilon_2 \varepsilon_6 \omega \lambda^2 \left(4-2A_0 + \frac{\varepsilon_5 B^*}{\varepsilon_7 \varepsilon_2 \varepsilon_6 \omega \lambda^2} \right)},$$

$$h_3 = -\frac{Ec Pr d^2 (\varepsilon_1 \varepsilon_4 \omega - \delta k_1 \varepsilon_6 (V_c \lambda + d))}{\omega^2 \left(4-2A_0 + \frac{\varepsilon_5 B^*}{\varepsilon_7 \varepsilon_2 \varepsilon_6 \omega \lambda^2} \right)}.$$

The local Nusselt number is specified by:

$$Nu = \frac{axq_w}{\kappa_f(T_w - T_\infty)} \tag{23}$$

where,

$$q_w = -\left(\kappa_f + \frac{16\sigma T_\infty^3}{3k^*} \right) \left(\frac{\partial T}{\partial y} \right)_{y=0} \tag{24}$$

On switching, Equation (23) in Equation (24), reduced *Nu* are found as:

$$\text{Re}_x^{-1/2} Nu = -\varepsilon_4(\varepsilon_5 + N_T)\theta_\eta(0) \tag{25}$$

Using Equation (22), The Nusselt number can be calculated easily.

4. Entropy Generation Analysis

In the existence of an MHD, the local volumetric rate of EG is given by:

$$S_G = \frac{\kappa_{nf}}{T_\infty^2} \left[\left(\frac{\partial T}{\partial x} \right)^2 + \left(1 + \frac{16\sigma^* T_\infty^3}{3k^* \kappa_f} \right) \left(\frac{\partial T}{\partial y} \right)^2 \right] + \frac{\mu_{nf}}{T_\infty} \left(\frac{\partial u}{\partial y} \right)^2 \frac{\sigma_{nf} B_0^2}{T_\infty} \text{Sin}^2 \tau u^2. \tag{26}$$

For the EG rate *N_G*, a dimensionless number is acceptable. The local volumetric EG rate *S_G* is divided by a typical entropy generation rate *S_{G0}* to get this figure. The characteristic entropy generation rate for a given boundary condition is:

$$S_{G0} = \frac{\kappa_f(\Delta T)^2}{l^2 T_\infty^2} \tag{27}$$

As a result, the number of entropy generation is:

$$N_S = \frac{S_G}{S_{G0}} \tag{28}$$

The entropy generation number is calculated using (21), (26), (27), and (28).

$$N_S = \varepsilon_5 \frac{4}{d^2} \theta^2(\eta) + \varepsilon_5 \text{Re}(1 + N_R) \theta_{\eta}^2(\eta) + \varepsilon_1 \text{Re} \frac{\Gamma}{\chi} f_{\eta\eta}^2(\eta) + \frac{\Gamma M}{\chi} f_{\eta}^2 \text{Sin}^2 \tau. \tag{29}$$

Here,

$$\text{Brinkman number } \Gamma = \frac{\mu u_p^2}{\kappa_f \Delta T},$$

temperature difference is $\chi = \frac{\Delta T}{T_{\infty}},$

5. Result and Discussion

The purpose of the work was to determine the impact of entropy production, nanofluid velocity, skin friction, temperature, and Nusselt number on numerous constraints. Here we were inspired by earlier published papers [35]. The current equation’s ODE was solved analytically, and the momentum equation, and the energy equation solved. This analytical solution was also employed in the energy equation, which was represented as a Kummer’s function with entropy analysis. Many technical processes involving hydromagnetic flows and thermal expansion in the porous medium have been studied in recent years, such as casting, compact heat exchangers, liquid metal filtering, fusion control, and nuclear reactor cooling. A uniform magnetic field acts perpendicular to the sheet, with a source of radiative heat and a convective condition at the boundary. The graphical arrangements given below can be used to facilitate the discussion. Although non-Newtonian fluids are extremely important and frequently used in science and industry, no attempt has been made to date to examine the Casson nanofluid flow with a permeable nonlinear stretching surface [37–40].

Figure 2 shows the influence of the M and the volume fraction on the non-dimensional velocity for stretching surface, while the other parameters are $\Lambda = V_c = d = 1$ and $\tau = 90^\circ$. As seen in the diagram, the Lorentz effect was reduced when raising the M decreased the thickness of the boundary layer, resulting in decreased shear stress on the wall. The reason for this was that when the magnetic parameter rose, the boundary layer decreased, which was accompanied by a decrease in the velocity gradient. In addition, the volume fraction reduced, and the boundary layer thickness reduced. This was in accordance with physical expectations, by which a magnetic field creates a resistive force that acts in the opposite direction to the fluid. As a result, a full examination of all of the effects would be exhaustive, requiring a massive amount of computing to be analytically evaluated for various parameter combinations.

The water-based CNTs are shown in Figure 3. For the inclined angle parameter and volume fraction parameters for stretching surface. and keeping other parameters as $\Lambda = V_c = M = d = 1$, nanofluid velocity and temperature profiles were created. By increasing the value of the inclined angle parameter, then, decreasing the value of the velocity profile, both volume fraction and inclination angle characteristics were improved.

Figure 4 depicts the effect of suction parameters and volume fraction on velocity profiles for the stretching sheet, keeping other parameters as $\Lambda = M = d = 1$ and $\tau = 90^\circ$. When increasing the value of volume fraction, the boundary layer decreased. Similarly, the same effect occurred when raising the value of the suction constraint as the velocity profiles of the SWCNT also decreased.

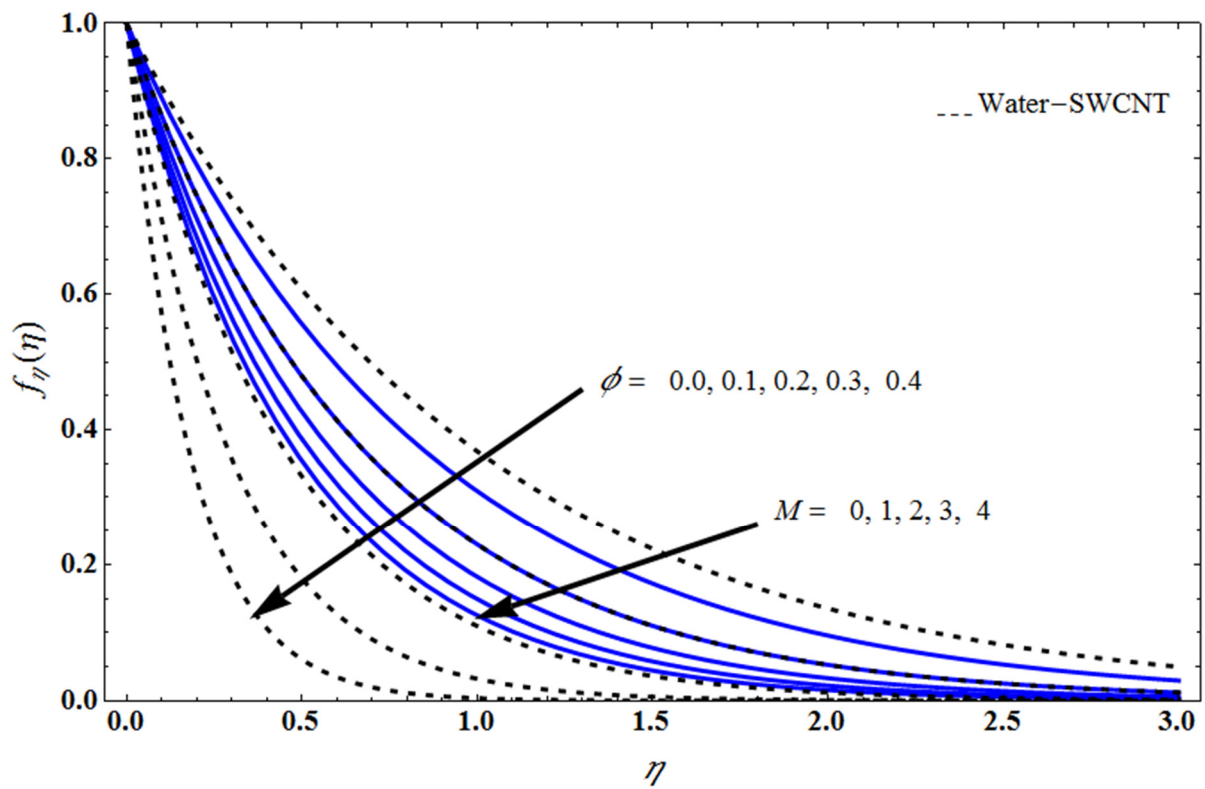


Figure 2. Impact of $f_{\eta}(\eta)$ on η for several values of M , and ϕ , respectively.

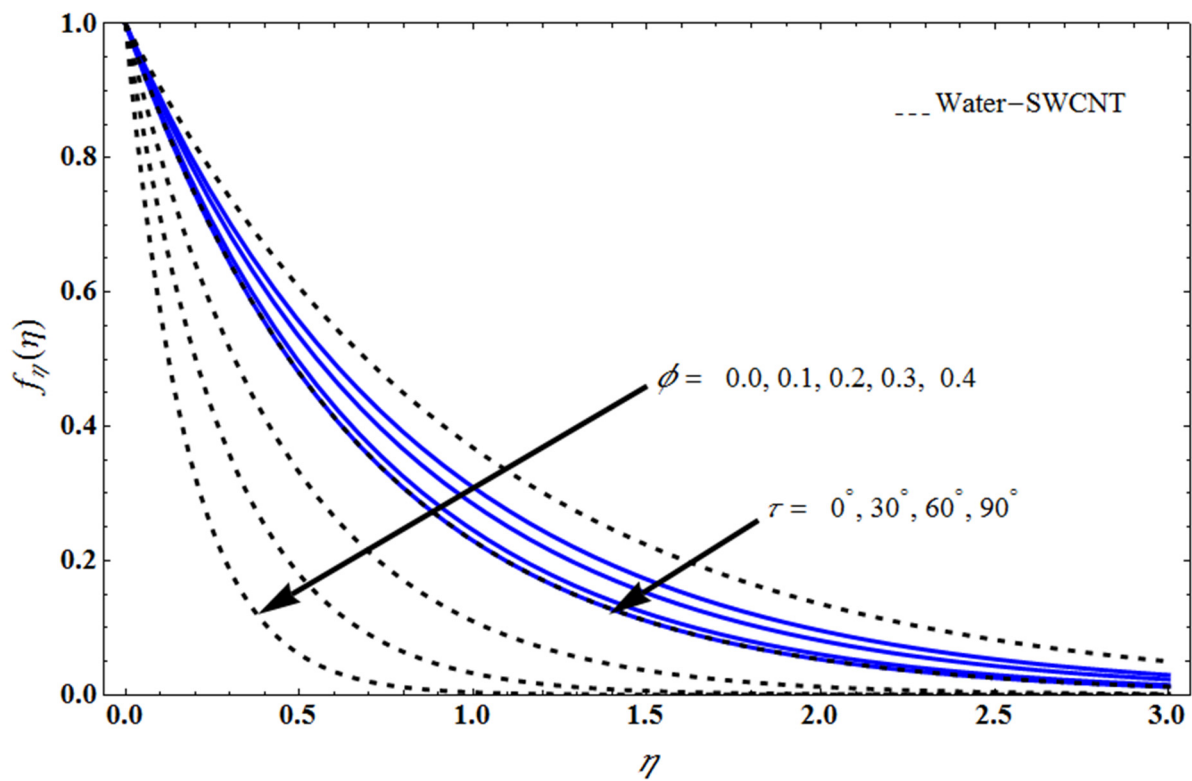


Figure 3. Effect of $f_{\eta}(\eta)$ on η for several values of τ , and ϕ , respectively.

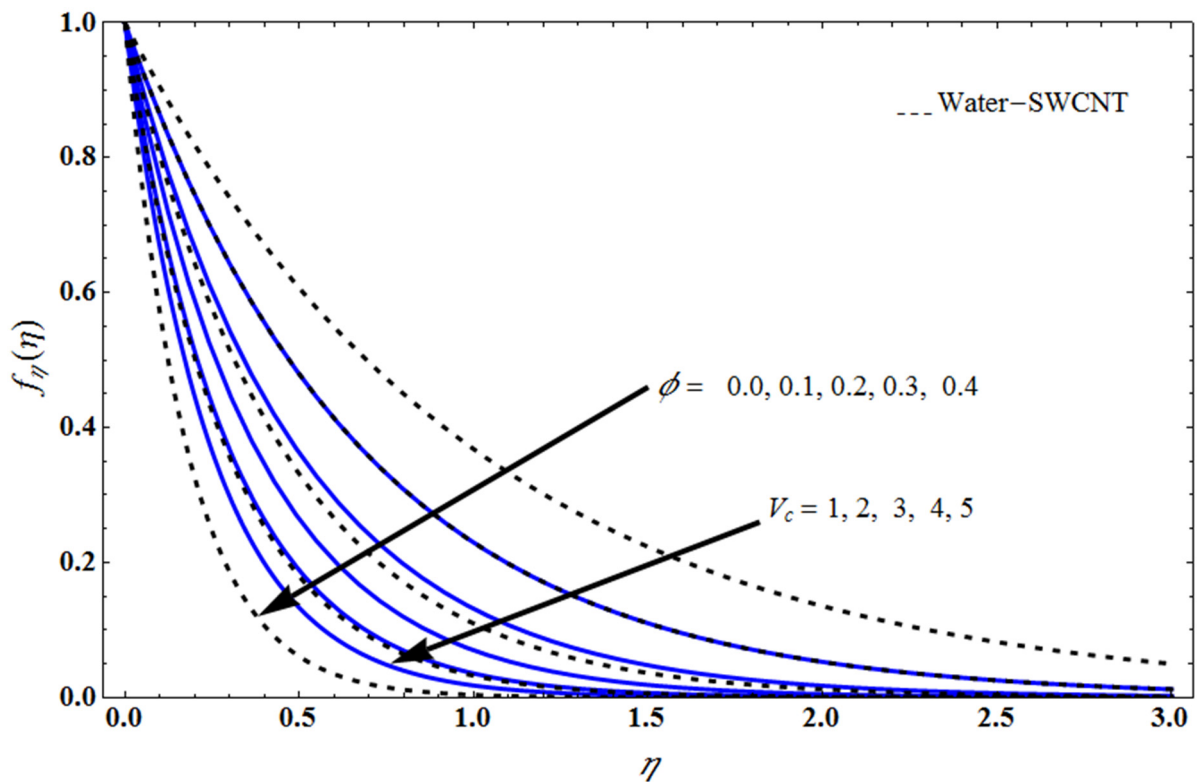


Figure 4. Effect of $f_\eta(\eta)$ on η for various values of V_c , and ϕ , respectively.

Figure 5 portrays the effect of suction parameters and Casson fluid parameter on the velocity profiles for stretching sheet, keeping other parameters as $M = d = 1$, $\phi = 0.1$ and $\tau = 90^\circ$. When increasing the Casson fluid constraint, the boundary layer thickness reduced. Increasing the value of the suction constraint also reduced the velocity profiles of the SWCNT. Physically, it is possible to claim that, as the Casson fluid parameter rose, it became difficult for the fluid to easily pass through, resistance to the fluid’s ability to move freely eventually reduced fluid velocity. Figure 6 displays the influence of the M on $\theta(\eta)$ for stretching surface, keeping other parameters as $\Lambda = V_c = d = N_R = k_1 = 1$, $Ec = 0.2$, $Pr = 6.2$, $\delta = 2$, $A^* = B^* = 0.1$ and $\tau = 90^\circ$. As seen in the diagram, raising the magnetic constraint reduced the thickness of the boundary layer. Here both SWCNT and MWCNT varied. The temperature distribution for various N_R is shown in Figure 7 for stretching surface. keeping other parameters as $\Lambda = V_c = d = 1$, $Pr = 6.2$, $\delta = 2$, $A^* = B^* = 0.1$ and $\tau = 90^\circ$ $M = k_1 = 1$, $Ec = 0.2$, . The boundary layer rose as the radiation of nanoparticles rose, as shown. Furthermore, as the N_R rose, the thermal boundary layer thickness rose. Subsequently, a dramatic temperature difference at the wall occurred and the heat transfer rate was faster. The strengthening of the radiation effect also meant that a large amount of thermal energy was transferred into the nanofluid. Thermal radiation thereby increased the thermal diffusivity of nanofluids; for emerging radiation parameter values, heat would be added to the regime, and temperatures would rise as a result. A fluid temperature greater than both the wall temperature and the surrounding ambient temperature is technically possible, as was mentioned for the heat transmission of flows over a stretching sheet. Here we have discussed forced flow over a stretching sheet. We now look at heat transport in the presence of radiation. The effect of heat conductivity is amplified by radiation. Radiation has the effect of dampening or enhancing heat transmission in a linear manner. Figure 8 displays the influence of the Ec on $\theta(\eta)$ for stretching surface, keeping other parameters as $\Lambda = V_c = d = N_R = k_1 = 1$, $M = 1$, $Pr = 6.2$, $\delta = 2$, $A^* = B^* = 0.1$ and $\tau = 90^\circ$. As seen in the diagram, increasing the Eckert number decreased the thickness of the boundary layer. Here both SWCNT and MWCNT varied. In terms of physics, significant frictional heating indicates that heat energy was stored in the

CNT, resulting in increased thermal boundary layer thickness. Figures 9 and 10 demonstrate the impact of heat source/sink parameter on the temperature profile for stretching sheet with CNTs. here $A^*, B^* > 0$ is heat production, and $A^*, B^* < 0$ is heat absorption. When the value of heat absorption constraint increased, the thickness of the thermal boundary layer reduced. Figure 11 displays the influence of an elastic deformation constraint on the temperature of CNTs. Increasing the elastic deformation decreased the thickness of the boundary layer. The existence of an elastic deformation consequence lowered heat energy transfer into the nanofluid. Figures 12–14 depict the influence of mass transpiration, Casson fluid and volume fraction on the skin friction coefficient. The skin friction coefficient rose as mass transpiration increased, and the skin friction coefficient rose if the Casson fluid was improved. The skin friction coefficient increased as the volume fraction increased, while the skin friction coefficient increased if the Casson fluid increased. Since increasing the value of mass transpiration means Casson fluid effects lower the surface, which, thus, reduce skin friction, and increasing the value of volume fraction effect increases skin friction in the CNTs. Results for carbon nanotubes with single and multiple walls were grouped and contrasted. According to our research, the Brinkman number and temperature ratio parameter rose together with entropy generation. Radiative factors became more intense as the temperature rose. Additionally, when compared to multiwall carbon nanotubes, the temperature gradient was slightly higher for single wall carbon nanotubes. Higher nanoparticle and suction parameter values improved skin friction.

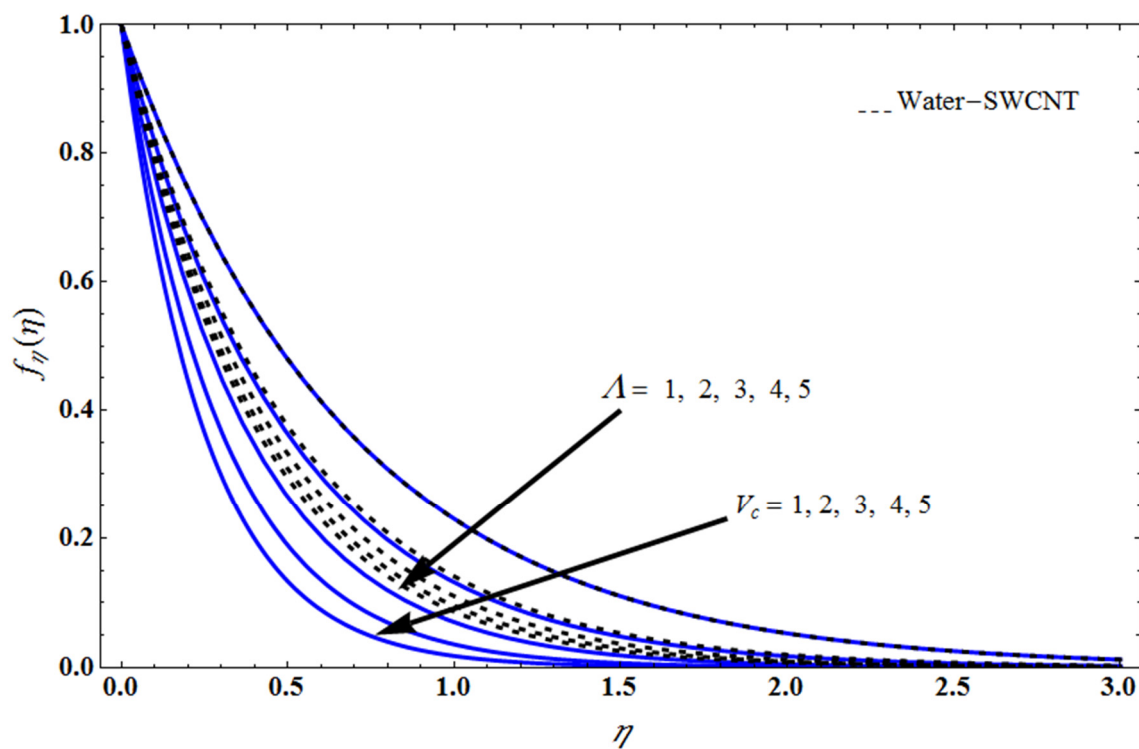


Figure 5. Effect of Axial velocity $f_{\eta}(\eta)$ versus similarity variable η for various values of mass transpiration V_c , and Λ , respectively.

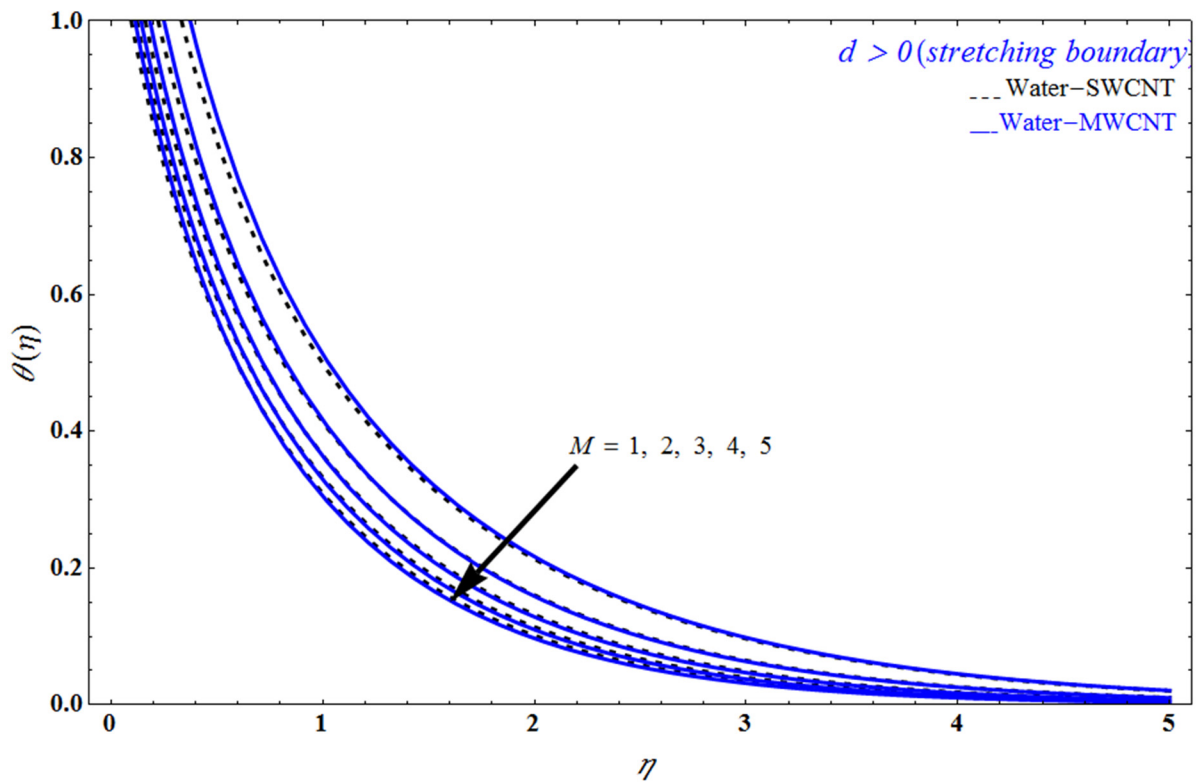


Figure 6. Effect of temperature profile $\theta(\eta)$ versus similarity variable η for several values of M , respectively.

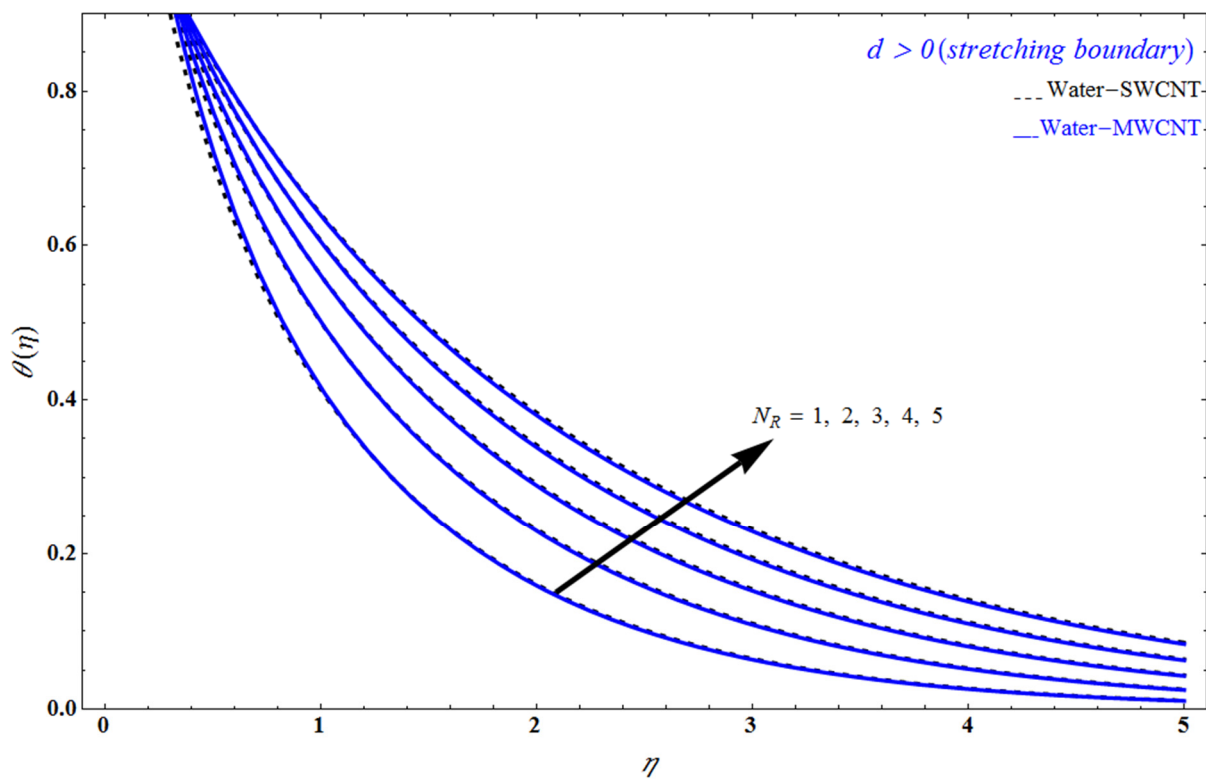


Figure 7. Effect of temperature profile $\theta(\eta)$ versus similarity variable η for several values of radiation N_R , respectively.

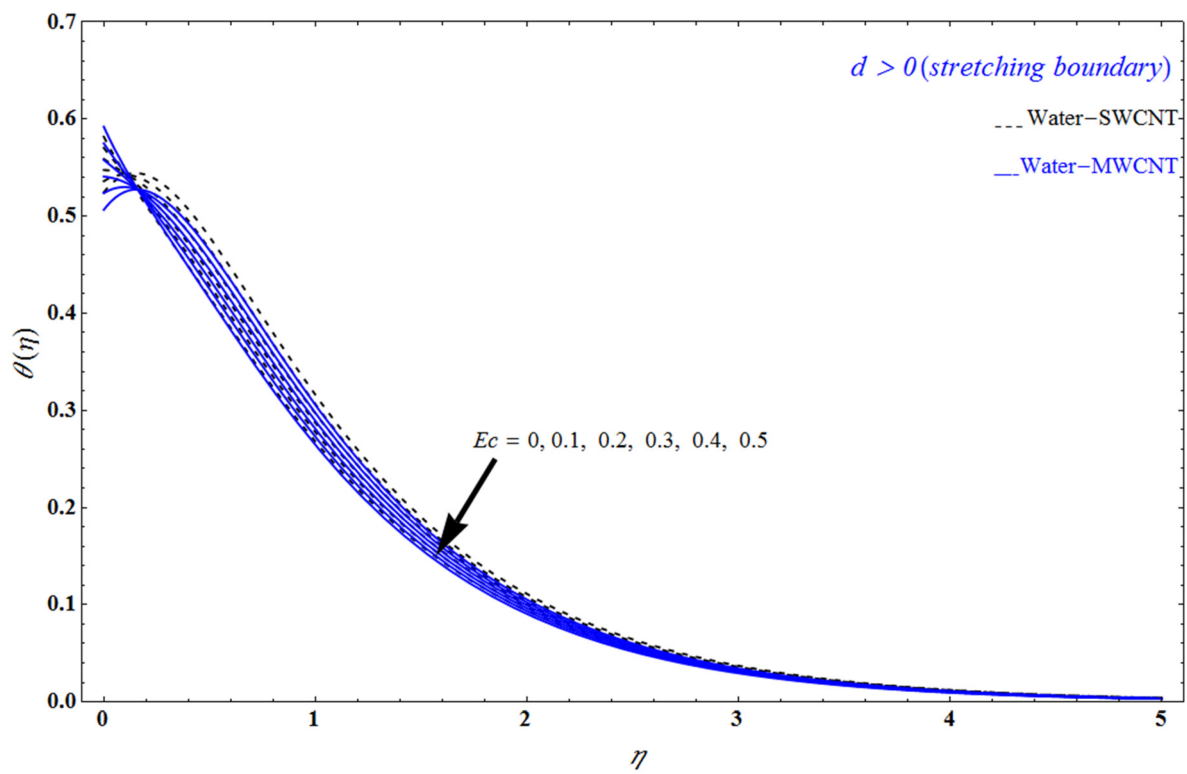


Figure 8. Effect of temperature profile $\theta(\eta)$ versus similarity variable η for several values of Ec , respectively.

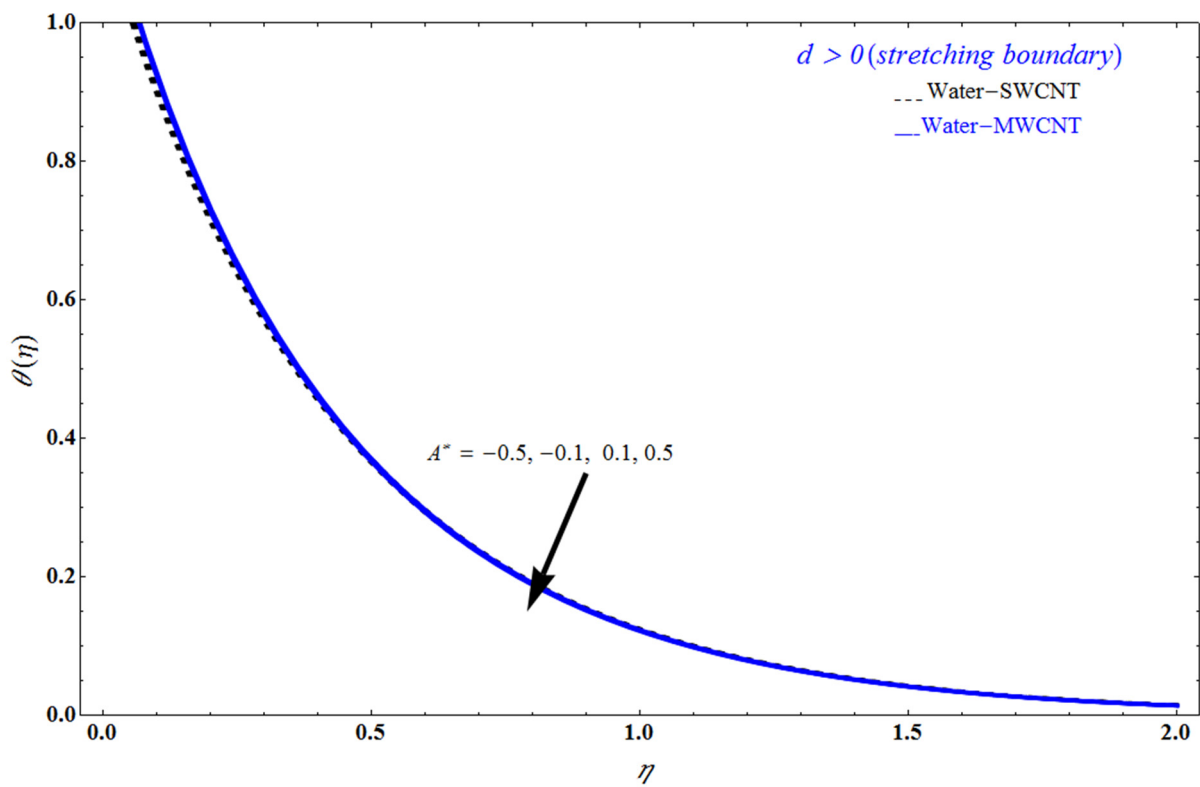


Figure 9. Impact of temperature profile $\theta(\eta)$ versus similarity variable η for several values of A^* , respectively.

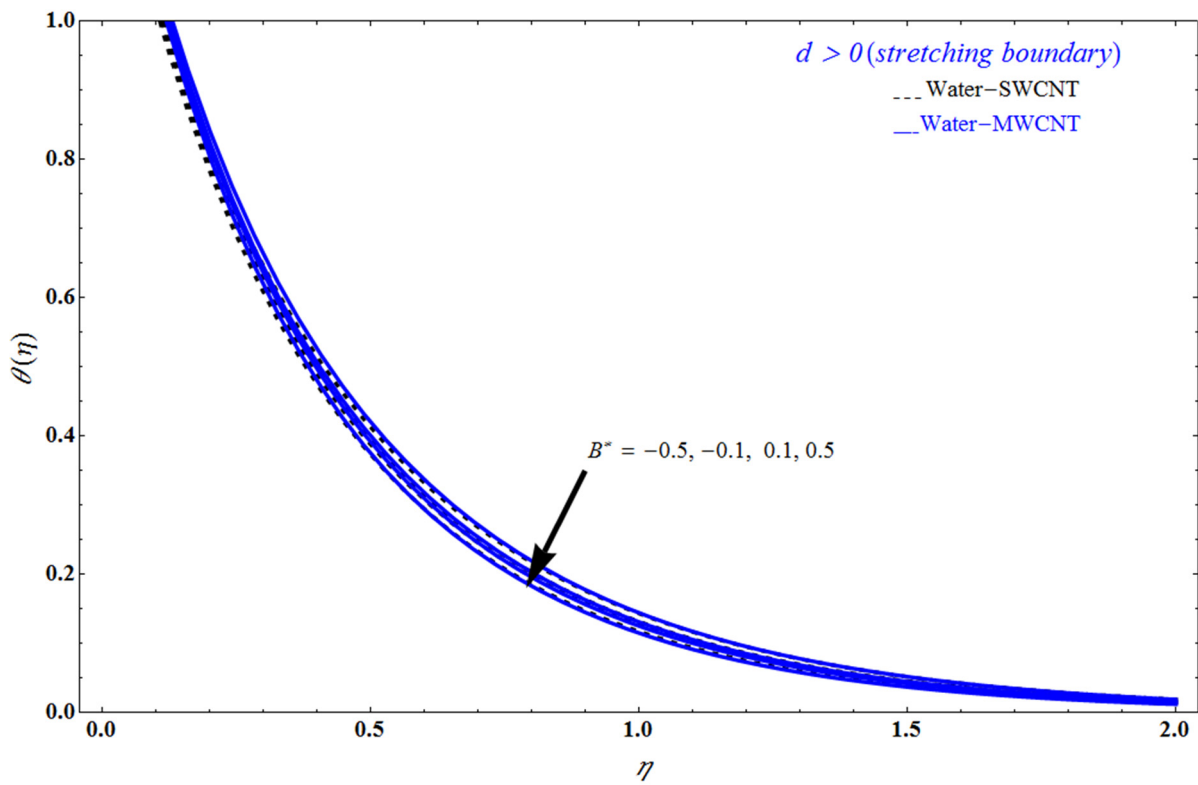


Figure 10. Impact of temperature profile $\theta(\eta)$ versus similarity variable η for numerous values of B^* , respectively.

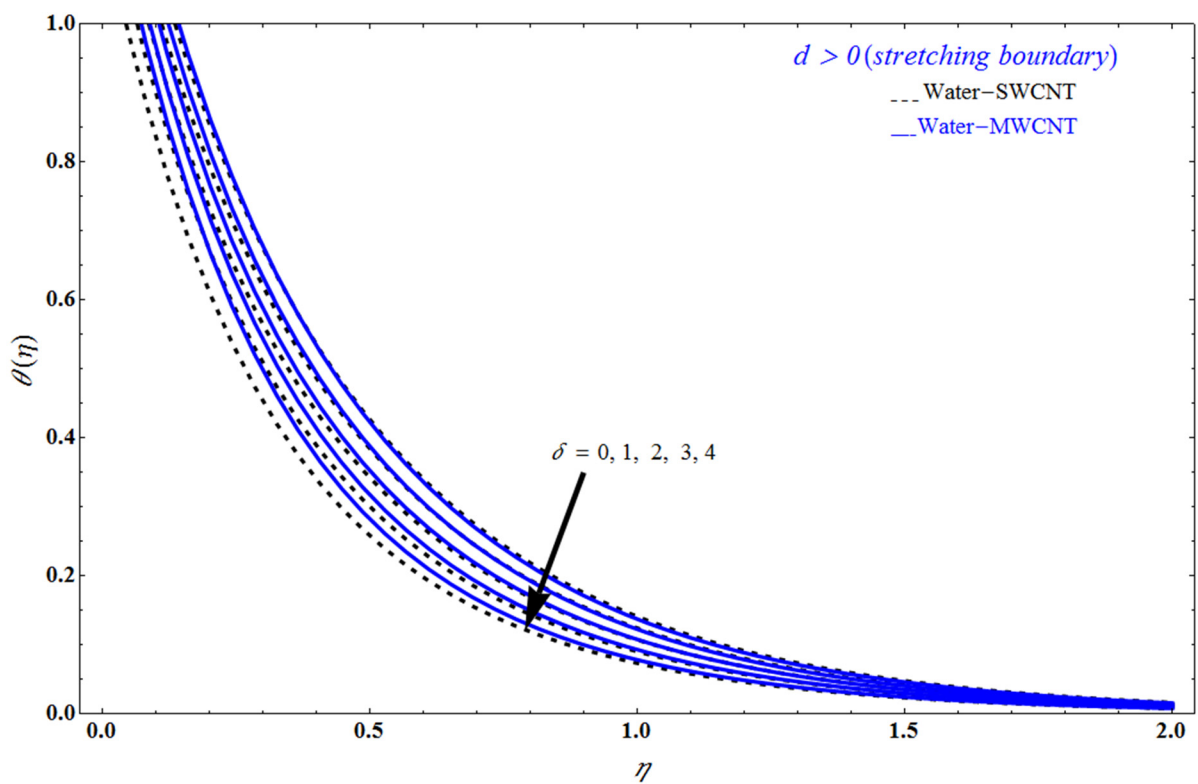


Figure 11. Impact of temperature profile $\theta(\eta)$ versus similarity variable η for several values of δ , respectively.

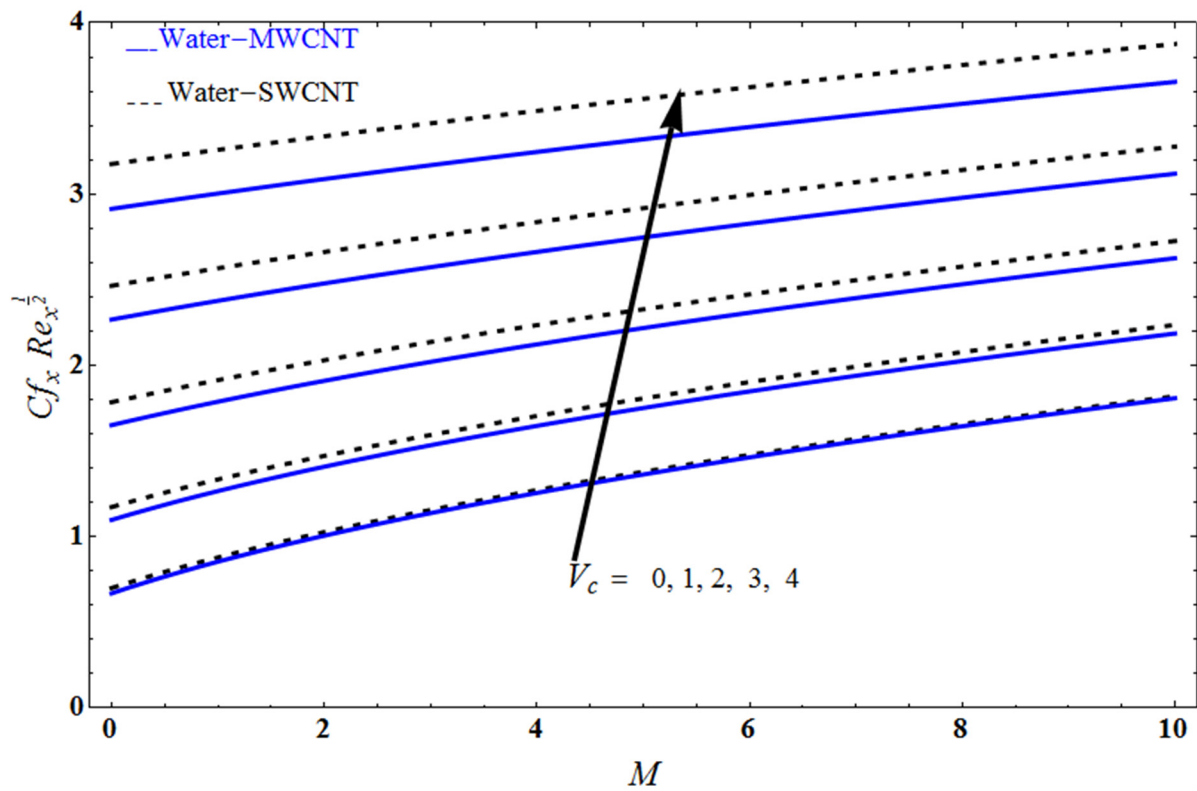


Figure 12. Impact of $Cf_x Re_x^{1/2}$ on M for several values of V_c , respectively.

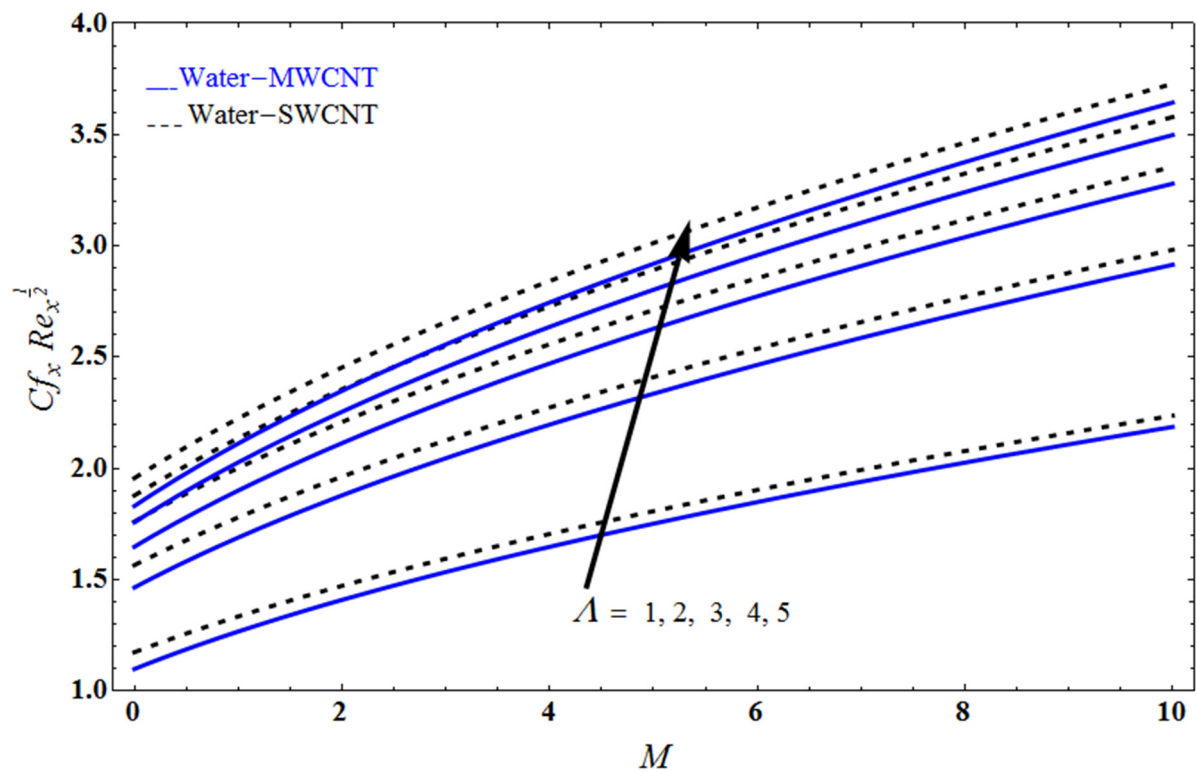


Figure 13. Impact of $Cf_x Re_x^{1/2}$ on M for several values of Λ , respectively.

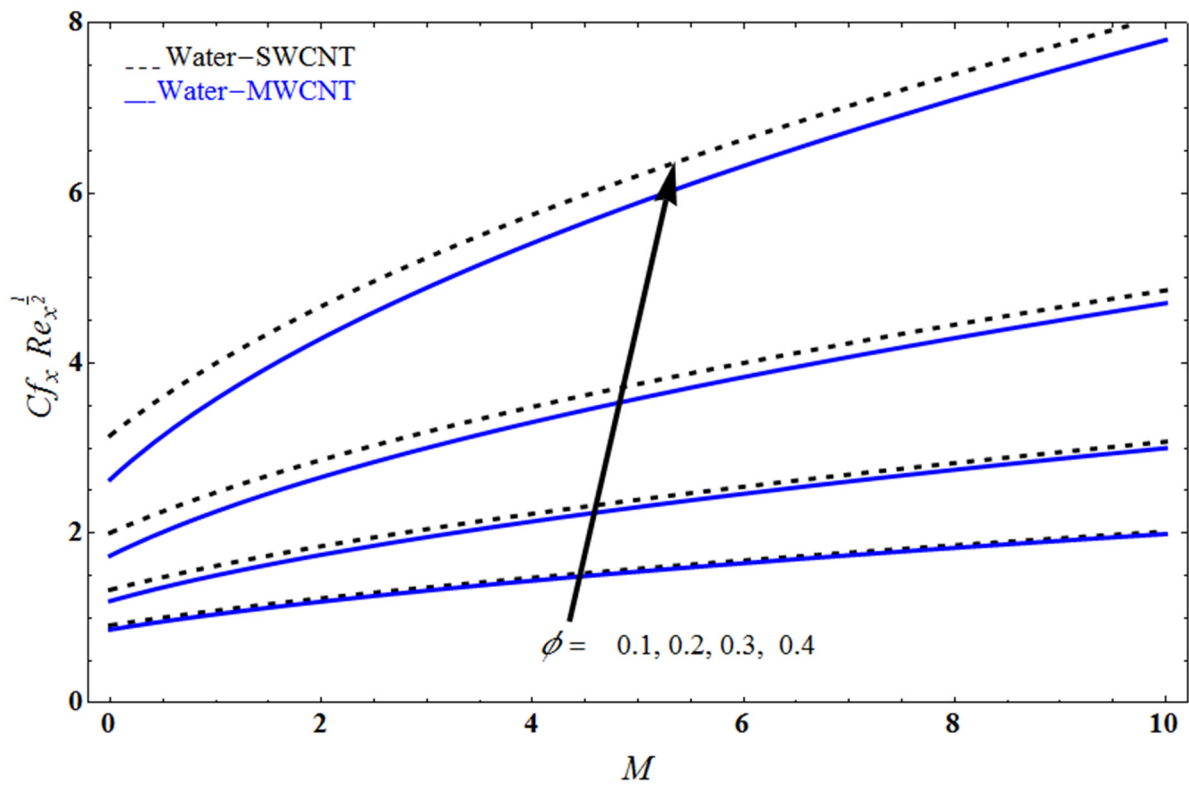


Figure 14. Impact of $Cf_x Re_x^{1/2}$ on M for several values of ϕ , respectively.

The Nusselt number versus elastic deformation parameter had an effect on the thermal radiation, and Eckert number, as shown in Figures 15 and 16. When the thermal radiation and Eckert number increased then the rate of heat transfer was observed to be enhanced.

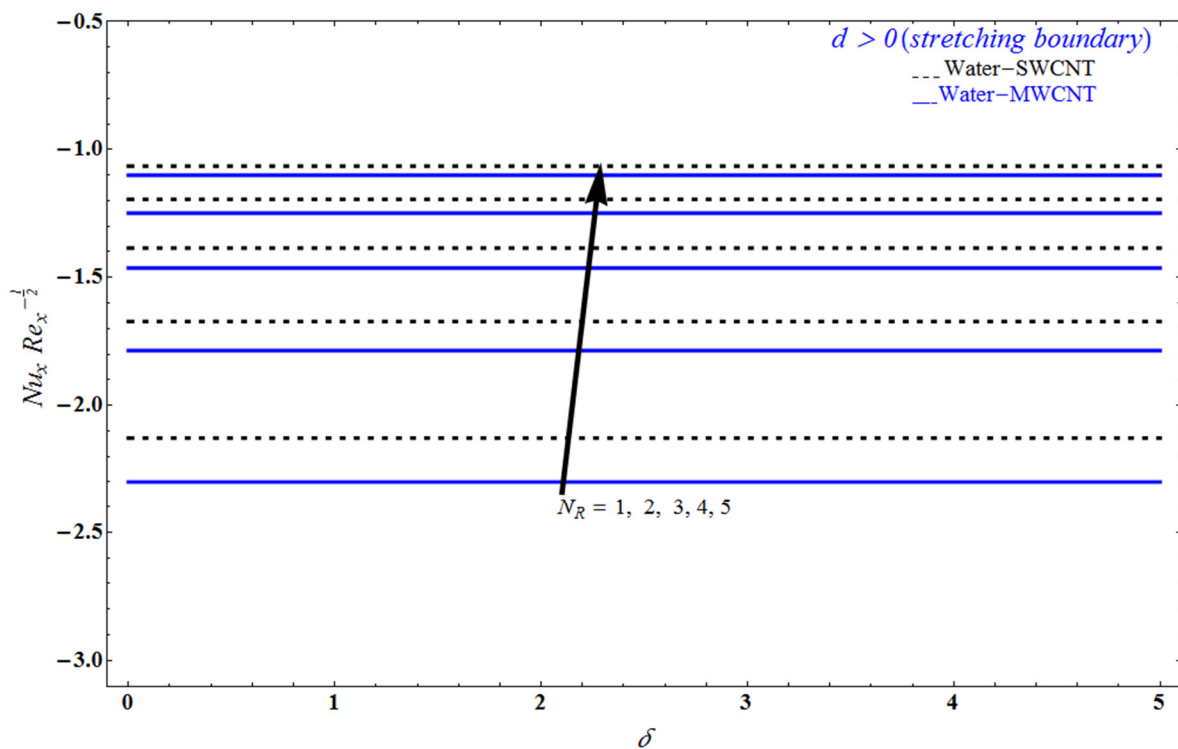


Figure 15. Impact of $Nu_x Re_x^{-1/2}$ on δ for several values of N_R , respectively.

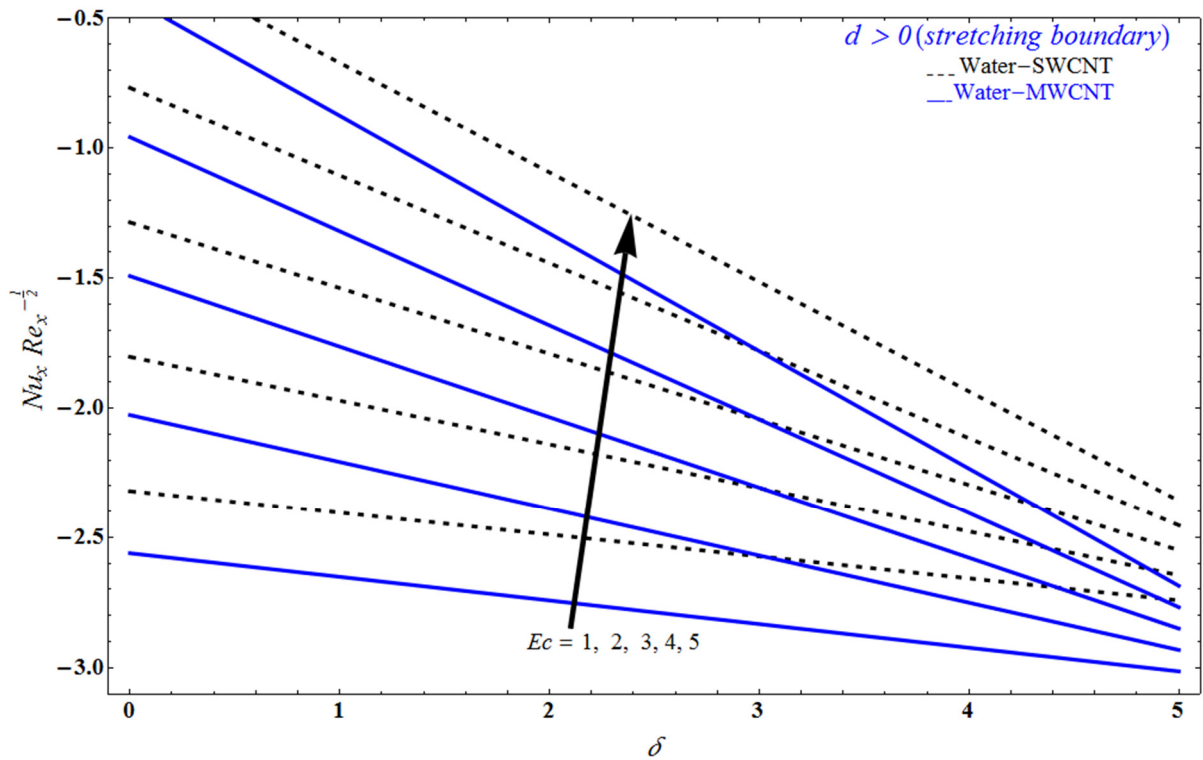


Figure 16. Impact of $Nu_x Re_x^{-1/2}$ on δ for several values of Ec , respectively.

Figures 17–19 illustrate the effect of entropy generation versus similarity variables for several values of elastic deformation constraint, Eckert number, and thermal radiation. When increasing the magnitude of elastic deformation, entropy increased. The presence of elastic deformation substantially affected the CNTs, resulting in higher entropy creation. Entropy production was minimized by both the Eckert number and the radiation constraints, although the opposite influence was demonstrated away from the wall. Since the rate of emission of heat energy near the sheet was lower in this location, entropy creation was minimized. Results for CNTs with single and multiple walls were grouped and contrasted. According to our research, the Brinkman number and temperature ratio parameter rose together with entropy generation. Radiative factors became more intense as the temperature rose. Additionally, when compared to MWCNT, the temperature gradient was slightly higher for SWCNT. Although non-Newtonian fluids are extremely important and frequently used in science and industry, no attempt has been made to date to examine the Casson nanofluid flow with a permeable nonlinear stretching surface. The findings show that radiation and dissipation effects increase entropy. Entropy can, therefore, be important in the artificial method used to analyze brain activity. The addition of nanoparticles to blood flow also increases warmth and velocity.

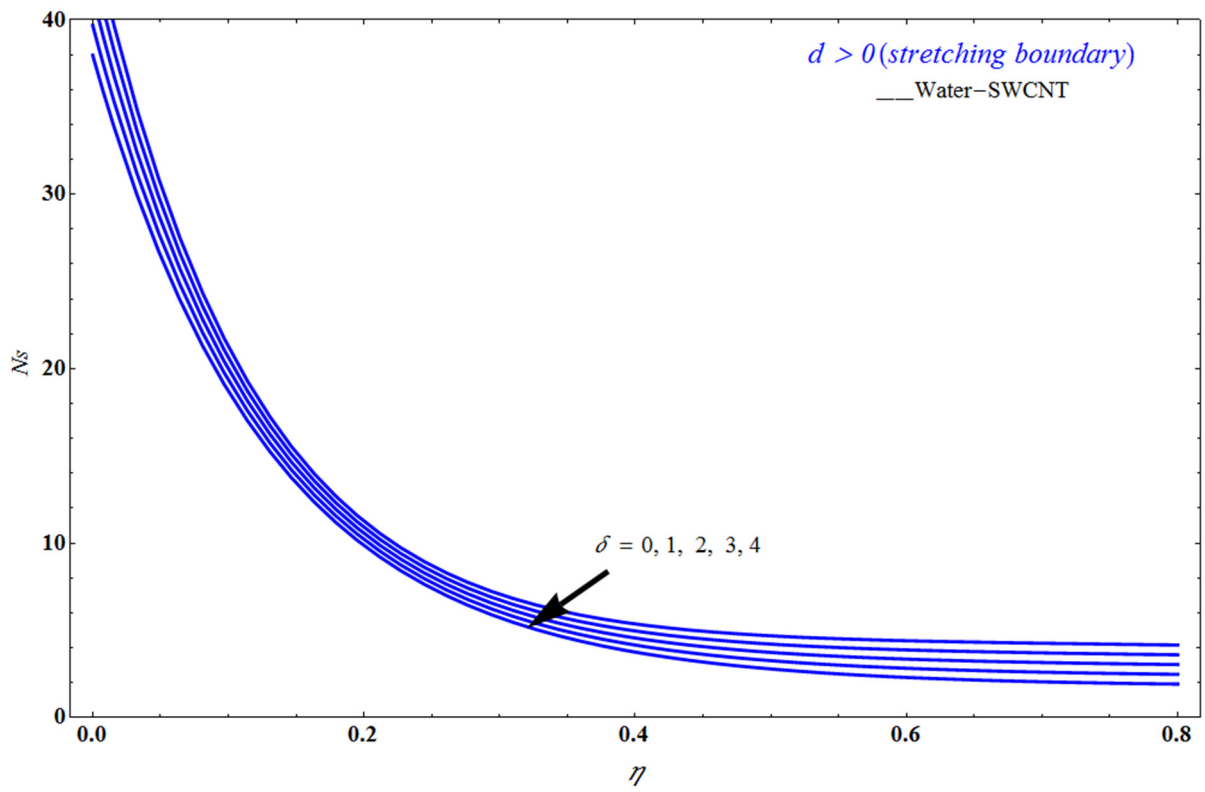


Figure 17. Influence of Ns on η for several values of δ , respectively.

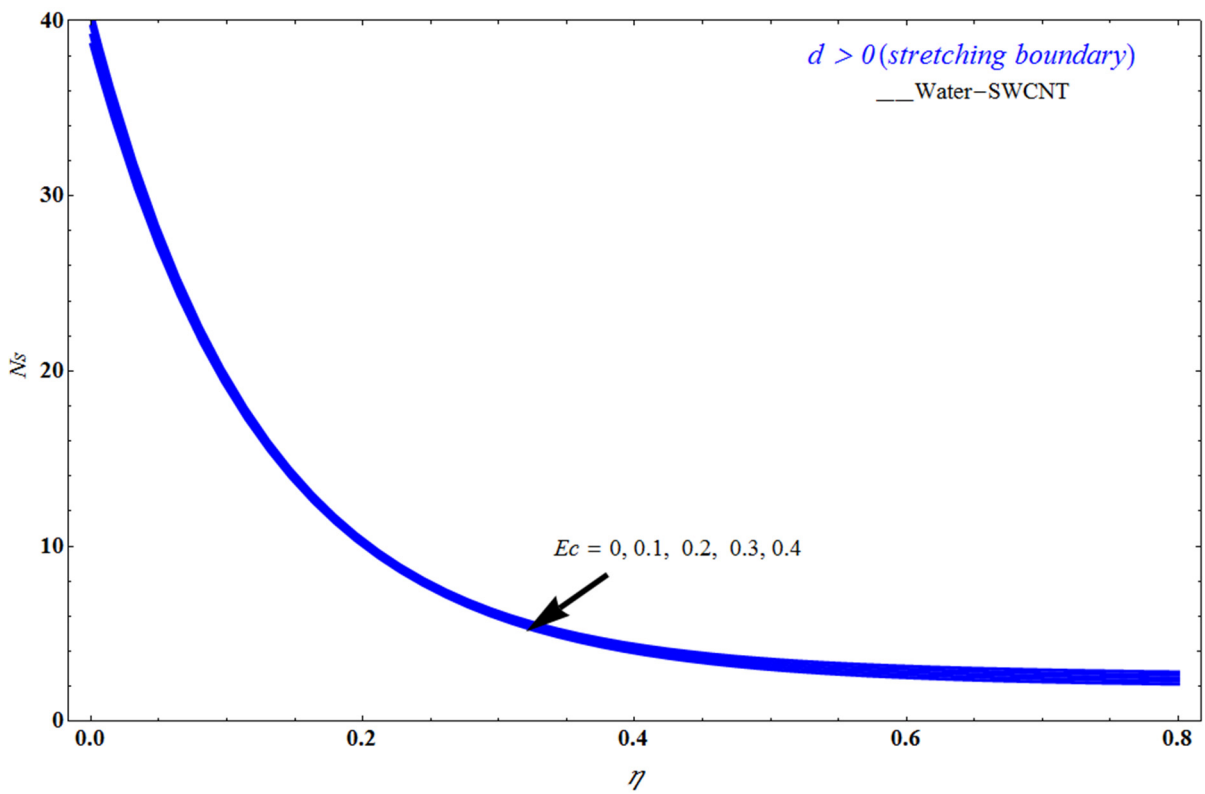


Figure 18. Influence of Ns on η for several values of Ec , respectively.

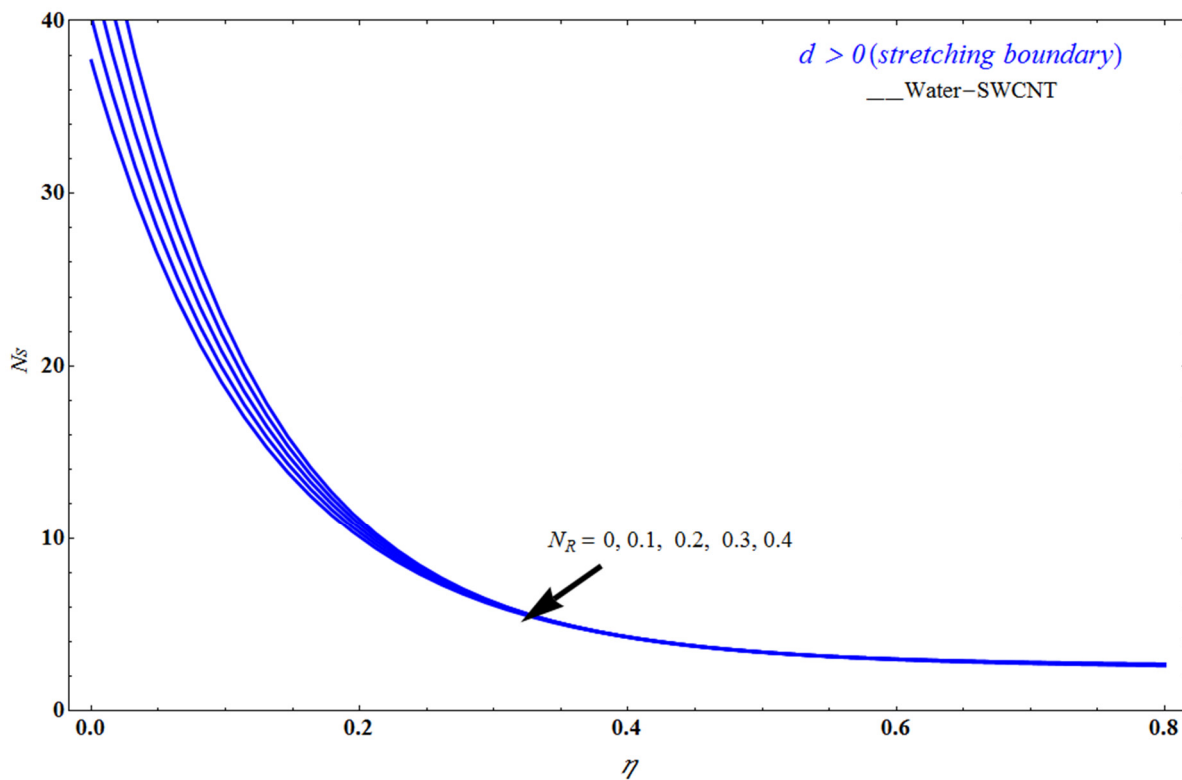


Figure 19. Impact of N_s on η for several values of N_R , respectively.

Here, we note that,

- i) The Crane flow [4] is recovered from Equation (15) for $\Lambda = N_R = 0$ and $\varepsilon_1 = \varepsilon_2 = \varepsilon_3 = \varepsilon_4 = 1$
- ii) The Pavlov flow [41] is recovered from Equation (15) for $\Lambda = N_R = 0$ and $\varepsilon_1 = \varepsilon_2 = \varepsilon_3 = \varepsilon_4 = 1$
- iii) The Mahabaleshwar et al. [42] flow is recovered from Equation (15) for $\Lambda = N_R = 0$ and $\varepsilon_1 = \varepsilon_2 = \varepsilon_3 = \varepsilon_4 = 1$

By comparing the present study to the works as shown in Table 3, the accuracy of the present study could be checked as follows:

- If $\Lambda = N_R = 0$ and $\varepsilon_1 = \varepsilon_2 = \varepsilon_3 = \varepsilon_4 = 1$, the current work for the stretched sheet scenario corresponded to the work of [23] in the absence of an inclined magnetic field.
- If $\Lambda = N_R = 0$, and $\varepsilon_1 = \varepsilon_2 = \varepsilon_3 = \varepsilon_4 = 1$, the current study agreed with recent findings by Mahabaleshwar et al. [42] when $\tau = \pi/2$ and $M = 1$.

Table 3. Comparison of present study and related works by other authors.

Related Works by Other Authors	Fluids	Value of α
Crane 1970, [4]	Newtonian	$\alpha = 1$
Pavlov 1974, [43]	Newtonian	$\alpha = \sqrt{1 + M}$
Siddheshwar et al. [44]	Non-Newtonian	$\alpha = \sqrt{\frac{1+M+K}{(1-k_1)}}$
Siddheshwar, and Mahabaleshwar [41]	Non-Newtonian	$\alpha = \sqrt{\frac{1+M}{(1-k_1)}}$
Present work	Non-Newtonian fluid	$F(\eta) = V_C + \frac{d}{\lambda}(1 - \text{Exp}(-\lambda\eta))$ $\lambda = \frac{V_C\varepsilon_2 + \sqrt{(2V_C\varepsilon_2)^2 - (d + \frac{\varepsilon_3}{\varepsilon_2} M \text{Sin}^2\tau) \frac{\varepsilon_1}{\varepsilon_2} (1 + \frac{1}{\lambda})}}{2 \frac{\varepsilon_1}{\varepsilon_2} (1 + \frac{1}{\lambda})}$ $F_{\eta\eta}(\eta) = -d\lambda \text{Exp}(-\lambda\eta)$

6. Conclusions

This paper presents an analytical analysis of EG for MHD of CNT across a stretched surface. The values of Nusselt and skin coefficients under several characteristics, such as magnetic field effects, Eckert number, mass transpiration, and nano particle volume fraction were studied in depth. According to the findings, introducing the base fluids in force reduced shear force and lowered the stretching sheet. With nanofluids, lower magnetic parameters and higher Eckert numbers resulted in better thermal conditions. The results for CNTs with single and multiple walls were grouped and contrasted. According to our research, the Brinkman number and temperature ratio parameter rose together with entropy generation. Radiative factors became more intense as the temperature rose. Additionally, when compared to MWCNT, the temperature gradient was slightly higher for SWCNT. Although non-Newtonian fluids are extremely important and frequently used in science and industry, no attempt has been made to date to examine the Casson nanofluid flow with a permeable nonlinear stretching surface. Furthermore, towards the surface, where considerable impermissibility exists, the rate of entropy generation was higher. The presences of various parameters, such as suction, magnetic field, and Casson fluids, were all slowed down by the CNT flow. Consequently, the momentum boundary layer’s thickness also reduced.

Author Contributions: Investigation, U.S.M.; Methodology, K.N.S.; Supervision, U.S.M., M.S. and M.H.A.; Writing—original draft, K.N.S.; Writing—review & editing, M.H.A. and M.A.-B. All authors have read and agreed to the published version of the manuscript.

Funding: This research received no external funding.

Data Availability Statement: Data sharing is not applicable to this article.

Conflicts of Interest: The authors declare no conflict of interest.

Nomenclature

List of Symbols	Definitions	SI Units
a	constants	$[s^{-1}]$
$A^* > 0$	non-uniform heat production	[-]
$A^* < 0$	non-uniform heat absorption	[-]
B_0	strength of magnetic field	$[W m^{-2}]$
$B^* > 0$	non-uniform heat production	[-]
$B^* < 0$	non-uniform heat absorption	[-]
b_0	constant	[-]
C_p	specific heat at constant pressure	$[J K^{-1} kg^{-1}]$
d	stretching parameter	[-]
f	similarity variable	[-]
k^*	mean absorption coefficient	$[m^{-2}]$
k_0	elastic parameter	[-]
M	Hartmann number	[-]
Pr	Prandtl number	[-]
q_r	radiative heat flux	$[J s^{-1} m^{-2}]$
q_w	heat flux at the wall	$[J s^{-1} m^{-2}]$
q'''	non-uniform heat generation/absorption	[-]
q_0	constant	[-]
N_R	radiation number	[-]
Re_x	local Reynolds number	[-]
T	temperature	[K]
T_∞	ambient temperature	[K]
T_w	surface temperature	[K]
u, v	velocity component	$[m s^{-1}]$
V_C	suction/injection	$[m s^{-1}]$
x, y	coordinate along the sheet	[m]

Greek symbols

α	thermal diffusivity	$[m^2 s^{-1}]$
λ	solution domain	[-]
Λ	Casson fluid	[-]
δ	elastic deformation	[-]
Γ	Brinkman number	[-]
χ	dimensionless temperature difference	[-]
κ	thermal conductivity	$[mol m^{-3}]$
ν	kinematic viscosity	$[m^2 s^{-1}]$
η	similarity variable	[-]
μ	dynamic viscosity	$[kg m^{-1} s^{-1}]$
ρ	density	$[kg m^{-3}]$
σ^*	Stefan-Boltzmann constant	$[Wm^{-2}K^{-4}]$
τ	inclined angle	[rad]
ϕ	volume fraction of nanoparticle	[-]

Subscript

f	base fluid	[-]
nf	nano fluid	[-]
w	wall condition	[-]
∞	For from the sheet	[-]

Abbreviations

B. Cs	boundary conditions	[-]
CNTs	carbon nanotubes	[-]
SWCNT	single-wall CNTs	[-]
MWCNT	multi-wall CNTs	[-]
MHD	magnetohydrodynamics	[-]
EG	Entropy generation	[-]

References

1. Fisher, E.G. *Extrusion of Plastics*, 3rd ed.; Newnes-Butterworld: London, UK, 1976; Volume 16, pp. 52–53.
2. Nandy, S.K. MHD Stagnation-Point Flow of Casson Fluid and Heat Transfer over a Stretching Sheet with Thermal Radiation. *J. Thermodyn.* **2013**, *9*, 169674.
3. Mabood, F.; Das, K. Outlining the impact of melting on MHD Casson fluid flow past a stretching sheet in a porous medium with radiation. *Heliyon* **2019**, *5*, e01216. [[CrossRef](#)] [[PubMed](#)]
4. Crane, L.J. Flow past a stretching plate. *Z. Angew. Math. Phys.* **1990**, *21*, 645–647. [[CrossRef](#)]
5. Andersson, H.; Bech, K.; Dandapat, B. Magnetohydrodynamic flow of a power-law fluid over a stretching sheet. *Int. J. Non-Linear Mech.* **1992**, *27*, 929–936. [[CrossRef](#)]
6. Andersson, H.I. MHD flow of a viscoelastic fluid past a stretching surface. *Acta Mech.* **1992**, *95*, 227–230. [[CrossRef](#)]
7. Fang, T.; Zhang, J. Closed-form exact solutions of MHD viscous flow over a shrinking sheet. *Commun. Non-Linear Sci. Numer. Simul.* **2009**, *14*, 2853–2857. [[CrossRef](#)]
8. Abolbashari, M.H.; Freidoonimehr, N.; Nazari, F.; Rashidi, M.M. Analytical modeling of entropy generation for Casson nano-fluid flow induced by a stretching surface. *Adv. Powder Technol.* **2015**, *26*, 542–552. [[CrossRef](#)]
9. Souayeh, B.; Reddy, M.G.; Sreenivasulu, P.; Poornima, T.; Rahimi-Gorji, M.; Alarifi, I.M. Comparative analysis on non-linear radiative heat transfer on MHD Casson nanofluid past a thin needle. *J. Mol. Liq.* **2019**, *284*, 163–174. [[CrossRef](#)]
10. Hakeem, A.A.; Renuka, P.; Ganesh, N.V.; Kalaivanan, R.; Ganga, B. Influence of inclined Lorentz forces on boundary layer flow of Casson fluid over an impermeable stretching sheet with heat transfer. *J. Magn. Magn. Mater.* **2016**, *401*, 354–361. [[CrossRef](#)]
11. Aly, E.H.; Pop, I. MHD flow and heat transfer near stagnation point over a stretching/shrinking surface with partial slip and viscous dissipation: Hybrid nanofluid versus nanofluid. *Powder Technol.* **2020**, *367*, 192–205. [[CrossRef](#)]
12. Aly, E.H.; Ebaid, A. MHD Marangoni boundary layer problem for hybrid nanofluids with thermal radiation. *Int. J. Numer. Methods Heat Fluid Flow* **2020**, *31*, 897–913. [[CrossRef](#)]
13. Anusha, T.; Mahabaleshar, U.S.; Sheikhejad, Y. An MHD of Nanofluid Flow Over a Porous Stretching/Shrinking Plate with Mass Transpiration and Brinkman Ratio. *Transp. Porous Media* **2021**, *142*, 333–352. [[CrossRef](#)]
14. Kumaran, G.; Sandeep, N. Thermophoresis and Brownian moment effects on parabolic flow of MHD Casson and Williamson fluids with cross diffusion. *J. Mol. Liq.* **2017**, *233*, 262–269. [[CrossRef](#)]
15. Iijima, S. Helical microtubules of graphitic carbon. *Nature* **1991**, *354*, 56–58. [[CrossRef](#)]
16. Khan, W.; Culham, R.; Haq, R.U. Heat Transfer Analysis of MHD Water Functionalized Carbon Nanotube Flow over a Static/Moving Wedge. *J. Nanomater.* **2015**, *2015*, 1–13. [[CrossRef](#)]

17. Anuar, N.S.; Norfifah, B.; Norihan, M.A.; Haliza, R. Mixed Convection Flow and Heat Transfer of Carbon Nanotubes over an Exponentially Stretching/Shrinking Sheet with Suction and Slip Effect. *J. Adv. Res. Fluid Mech. Therm. Sci.* **2019**, *59*, 232–242.
18. Khan, W.A.; Khan, Z.H.; Rahi, M. Fluid flow and heat transfer of carbon nanotubes along a flat plate with Navier slip boundary. *Appl. Nanosci.* **2014**, *4*, 633–641. [[CrossRef](#)]
19. Shalini, J.; Manjeet, K.; Amit, P. Unsteady MHD chemically reacting mixed convection nano-fluids flow past an inclined porous stretching sheet with slip effect and variable thermal radiation and heat source. *Sci. Direct* **2018**, *5*, 6297–6312.
20. Yana, S.R.; Mohsen, I.; Mikhali, A.S.; Ioan, I.; Hakan, F.; Oztope, M.A. Inclined Lorentz force impact on convective-radiative heat exchange of micropolar nanofluid inside a porous enclosure with tilted elliptical heater. *Int. Commun. Heat Mass Transf.* **2020**, *117*, 104762. [[CrossRef](#)]
21. Mukhopadhyay, S.; Vajravelu, K. Diffusion of chemically reactive species in Casson fluid flow over an unsteady permeable stretching surface. *J. Hydrodyn.* **2013**, *25*, 591–598. [[CrossRef](#)]
22. Sankar, D.; Lee, U. Two-fluid Casson model for pulsatile blood flow through stenosed arteries: A theoretical model. *Commun. Non-Linear Sci. Numer. Simul.* **2010**, *15*, 2086–2097. [[CrossRef](#)]
23. Sneha, K.N.; Mahabaleswar, U.S.; Chan, A.; Hatami, M. Investigation of radiation and MHD on non-Newtonian fluid flow over a stretching/shrinking sheet with CNTs and mass transpiration. *Waves Random Complex Media* **2022**, *11*, 1–20. [[CrossRef](#)]
24. Bejan, A. The Method of Entropy Generation Minimization. In *Energy and the Environment*; Springer: Dordrecht, The Netherlands, 1999; pp. 11–22. [[CrossRef](#)]
25. Khan, M.I.; Hafeez, M.; Hayat, T.; Khan, M.I.; Alsaedi, A. Magnetorotating flow of hybrid nanofluid with entropy generation. *Comput. Methods Programs Biomed.* **2020**, *183*, 105093. [[CrossRef](#)] [[PubMed](#)]
26. Shafee, A.; Haq, R.U.; Sheikholeslami, M.; Herki, J.A.A.; Nguyen, T.K. An entropy generation analysis for MHD water based Fe₃O₄ ferrofluid through a porous semi annulus cavity via CVFEM. *Int. Commun. Heat Mass Transf.* **2019**, *108*, 104295. [[CrossRef](#)]
27. Jamshed, W.; Aziz, A. Cattaneo–christov based study of tio 2-cuo/eg casson hybrid nanofluid flow over a stretching surface with entropy generation. *Appl. Nanosci.* **2018**, *8*, 685–698. [[CrossRef](#)]
28. Sindhu, S.; Gireesha, B. Entropy generation analysis of hybrid nanofluid in a microchannel with slip flow, convective boundary and nonlinear heat flux. *Int. J. Numer. Methods Heat Fluid Flow* **2019**, *3*, 53–74. [[CrossRef](#)]
29. Khan, M.I.; Qayyum, S.; Kadry, S.; Khan, W.A.; Abbas, S.Z. Irreversibility Analysis and Heat Transport in Squeezing Nanoliquid Flow of Non-Newtonian (Second-Grade) Fluid Between Infinite Plates with Activation Energy. *Arab. J. Sci. Eng.* **2020**, *45*, 4939–4947. [[CrossRef](#)]
30. Mumraiz, S.; Ali, A.; Awais, M.; Shutaywi, M.; Shah, Z. Entropy generation in electrical magnetohydrodynamic flow of Al₂O₃/Cu-H₂O hybrid nanofluid with non-uniform heat flux. *J. Therm. Anal. Calorim.* **2021**, *143*, 2135–2148. [[CrossRef](#)]
31. Reddy, P.B.A. Biomedical aspects of entropy generation on electromagnet hydrodynamic blood flow of hybrid nanofluid with nonlinear thermal radiation and non-uniform heat source/sink. *Eur. Phys. J. Plus* **2020**, *135*, 852. [[CrossRef](#)]
32. Hayat, T.; Tamoor, M.; Khan, M.I.; Alsaedi, A. Numerical simulation for nonlinear radiative flow by convective cylinder. *Results Phys.* **2016**, *6*, 1031–1035. [[CrossRef](#)]
33. Sneha, K.N.; Mahabaleswar, U.S.; Bennacer, R.; Ganaoui, M.E. Darcy Brinkman Equations for Hybrid Dusty Nanofluid Flow with Heat Transfer and Mass Transpiration. *Computation* **2021**, *9*, 118. [[CrossRef](#)]
34. Vishalakshi, A.B.; Mahabaleswar, U.S.; Sarris, I.E. An MHD Fluid Flow over a Porous Stretching/Shrinking Sheet with Slips and Mass Transpiration. *Micromachines* **2022**, *13*, 116. [[CrossRef](#)] [[PubMed](#)]
35. Xue, Q.Z. Model for thermal conductivity of carbon nanotube-based composites. *Phys. B Condens. Matter* **2005**, *368*, 302–307. [[CrossRef](#)]
36. Anuar, N.S.; Bachok, N.; Turkyilmazoglu, M.; Arifin, N.M.; Rosali, H. Analytical and stability analysis of MHD deforming vertical surface in carbon nanotubes. *Alex. Eng. J.* **2020**, *59*, 497–507. [[CrossRef](#)]
37. Ali, L.; Ali, B.; Ghori, M.B. Melting effect on Cattaneo–Christov and thermal radiation features for aligned MHD nanofluid flow comprising microorganisms to leading edge: FEM approach. *Comput. Math. Appl.* **2022**, *109*, 260–269. [[CrossRef](#)]
38. Ali, L.; Ali, B.; Liu, X.; Iqbal, T.; Zulqarnain, R.M.; Javid, M. A comparative study of unsteady MHD Falkner–Skan wedge flow for non-Newtonian nanofluids considering thermal radiation and activation energy. *Chin. J. Phys.* **2022**, *77*, 1625–1638. [[CrossRef](#)]
39. Ali, L.; Ali, B.; Liu, X.; Ahmed, S.; Shah, M.A. Analysis of bio-convective MHD Blasius and Sakiadis flow with Cattaneo–Christov heat flux model and chemical reaction. *Chin. J. Phys.* **2022**, *77*, 1963–1975. [[CrossRef](#)]
40. Ali, L.; Liu, X.; Ali, B.; Abdal, S.; Zulqarnain, R.M. Finite element analysis of unsteady MHD Blasius and Sakiadis flow with radiation and thermal convection using Cattaneo–Christov heat flux model. *Phys. Scr.* **2021**, *96*, 125219. [[CrossRef](#)]
41. Siddheshwar, P.; Mahabaleswar, U. Effects of radiation and heat source on MHD flow of a viscoelastic liquid and heat transfer over a stretching sheet. *Int. J. Non-Linear Mech.* **2005**, *40*, 807–820. [[CrossRef](#)]
42. Mahabaleswar, U.S.; Anusha, T.; Sakanaka, P.H.; Bhattacharyya, S. Impact of inclined Lorentz force and Schmidt number on chemically reactive Newtonian fluid flow on a stretchable surface when Stefan blowing and thermal radiation are significant. *Arab. J. Sci. Eng.* **2021**, *46*, 12427–12443. [[CrossRef](#)]
43. Pavlov, K.B. Magnetohydrodynamic flow of an incompressible viscous liquid caused by deformation of plane surface. *Magn. Gidrodin.* **1974**, *4*, 146–147.
44. Siddheshwar, P.G.; Chan, A.; Mahabaleswar, U.S. Suction-induced magnetohydrodynamics of a viscoelastic fluid over a stretching surface within a porous medium. *IMA J. Appl. Math.* **2014**, *79*, 445–458. [[CrossRef](#)]